Response to anonymous referee #1

The manuscript by Welles et al addresses an important need which is the comparison of top-down and bottom-up estimates of global N2O emissions. The authors are comparing several approaches to construct the initial conditions and proposed 'novel dimension reduction technique employing randomized singular value decomposition (SVD)' as a new aggregation technique. The manuscript is very well written and contributes to this research topic. The only concerns I have relate to the interpretation of results. A range of possible reasons for discrepancies in the a priori and a posteriori results are not considered even though these are mentioned in the Introduction. In addition, I think a direct comparison with the recent spatially resolved bottom up approach by Gerber et al. (2016) (see reference listed below) is needed. I have given some specific suggestions for improvements below.

We wish to thank the reviewer for their positive evaluation of our manuscript. Please find our responses to specific comments below, where the comment is in italics and our response is in bold.

Title: 'optimal resolution': this term is mentioned in Introduction and M&M, but not in Abstract/Conclusions. Perhaps it can be added to provide connections for reader.

Thank you for the suggestion. We have added the term "optimal resolution" in the abstract and in the conclusions.

Page 1 L. 19: Is a comma needed here 'global, monthly'?

We have deleted this comma, as well as another separating the same words in the conclusions.

L. 29: 'more' than? Please clarify.

The word "more" here referred to the a priori database. We have deleted the word and left "consistent with" to avoid confusion.

L. 30: 'fertilizer': I assume authors are referring to inorganic fertilizer (as in main text) but N2O emissions are driven by all forms of N input (manure, crop residue, soil mineralization, wet and dry N deposition. Manure addition could also be contributing to the seasonality.

Thank you for pointing this out. We have clarified this in the abstract as "spring fertilizer and manure application".

L. 32: Please see my comments for this explanation below.

L. 33: 'aliasing': this term is not used elsewhere in the text. It would be helpful to use term consistently so connections between different sections of manuscript can be made.

Thanks for the suggestion. We have changed the word "aliasing" to "biasing" to be more consistent with terms used elsewhere.

Page 2 L. 9-10: '... attribution of the source to specific regions and sectors is hindered by the strong spatio-temporal variability in N2O emissions…': something seems amiss here. High spatial variability hinders source attribution to regions? Do you mean 'Sources ARE highly variable in space and time and this hinders top-down approaches because of…(factors listed in remaining text)?

We have now reworded this sentence for greater clarity.

L. 21: Manure N use also increased as shown by Davidson 2009 (cited here).

We have now included manure N in this sentence.

L. 25: indirect N2O emissions are also due to NH3 volatilization; please include a reference to this.

Thank you for pointing out this omission. We now mention indirect emissions due to deposition of volatilized NO_x and NH_3 here in the text.

L. 26: It is not just uncertainties in the indirect component that affect the global N2O budget. The non-linear response to N input rates (please see Gerber et al. 2016, Spatially explicit estimates of N2O emissions from croplands suggest climate mitigation opportunities from improved fertilizer management, GCB), uncertainties in manure management estimates (e.g. manure deposited in pasture), and soil freeze/thaw effects are some examples of aspects that should be cited here.

Indeed, we did not mean to imply here that the indirect emissions are the only source of uncertainty in the global agricultural N_2O budget. To that end, we now include a sentence here saying: "These sources are all subject to large uncertainties. For example…"" We already mention the nonlinear response to N input rates two sentences earlier. We have now also added a sentence specifically referencing Gerber et al. (2016) and the under or overestimate that can arise

due to the non-linear response of emissions to fertilizer application. Freeze/thaw effects are already addressed in the following paragraph.

L. 26: Omit 'a body of' as two studies do not seem to warrant this statement. In addition, the factors cited above (non-linear response, freeze/thaw, etc.) also point to over or under-estimates (depending on factor) and these should be mentioned here.

We have deleted "a body of" from this sentence. Uncertainties in these other factors are now more explicitly addressed as described in our response to the previous comment.

Page 3 L. 2: when fertilizer is applied is not necessarily the issue unless it coincides with favourable soil conditions. It may be useful to mention wet/dry cycles here (see Kim et al. 2012, Effects of soil rewetting and thawing on soil gas fluxes: a review of current literature and suggestions for future research, Biogeosci.) and how they interact with management of N input.

This sentence did not say that fertilizer application timing was the main issue, just that microbial nitrification and denitrification depends on fertilizer application in general. In response to the reviewer's comment, we have now changed the wording to the following, and added a reference to Kim et al.: "Because microbial nitrification and denitrification, and the subsequent soil-atmosphere N_2O flux, depend strongly on factors such as soil moisture, temperature, physical characteristics, and N availability (e.g., Potter et al., 1996; Bouwman, 1998; Kim et al., 2012; Bouwman et al., 2013; Butterbach-Bahl et al., 2013; Griffis et al., 2017), N_2O emissions can exhibit major temporal and spatial variability."

L. 4: I do not recall that this paper looked at duration of freeze-thaw cycles. From what I recall it is showing the global agric N2O budget could be underestimated by a certain amount due to these cycles. This seems to be the relevant aspect of that publication to cite here.

This paper estimated a global N_2O source during the non-growing season due to short-duration thaw events in seasonally frozen soils. Adding this to the current EDGAR direct source for these soils results in the 35-65% contribution cited. We have clarified in the text that this contribution is to the direct source, and added some text to mention what the total global agricultural underestimation could be: "For example, Wagner-Riddle et al. (2017) found that short-duration freeze-thaw cycles can account for 35-65% of the annual direct N_2O emissions from seasonally

frozen croplands, and that neglecting this contribution would lead to a 17-28% underestimate of the global N_2O source (direct+indirect) from agricultural soils."

L. 32: I may have missed something but the airborne measurements were not used to directly assess optimized emissions, correct?

Correct. This is mentioned in Section 2.3 and in the caption of Fig. 4, but we have also added the word "independent" before "airborne measurements" here as a reminder that these were not used in the inversion.

Page 4 L. 6: Why was this period chosen for simulation?

N_2O measurements started at the KCMP tall tower in April 2010, so our simulation period spans the first two years of observations at that site. We have added this explanation here.

L. 15: Should mention that monthly values for N2O emissions from Edgar were used. Need to discuss here and/or later what drives the seasonal variation in this model and how/why it does not capture some of the seasonal variation discussed in Intro.

We use annual emissions from EDGAR in our a priori. We have added the word "annual" here as a reminder, and have added some text when discussing the seasonality to note that the (monthly) natural soil source is driving the seasonality of emissions over land.

Page 9 L. 11 'Remoteopt' used only observations from the remote sites, correct?

Correct. We have clarified this here as follows: "Three involve interpolation of surface observations from the NOAA, AGAGE, CSIRO, EC, and NIWA networks for alternate time windows (MarZonal, AprZonal, AprKriging), two involve 4D-Var adjoint optimization of the initial mass field based on those same observations plus those from KCMP tall tower (AprOpt, FebOpt), and one involves optimization of the initial mass field based on observations from remote sites (RemoteOpt)."

L. 21: 'remote sites': it would be helpful to list which ones are remote sites, here and/or in table heading.

Thanks for the suggestion. We have added a footnote to the table denoting which sites were considered remote.

L. 26: Should mention evaluation was done for each hemisphere (as shown in table 2).

We have added this clarification as follows: "Table 2 shows initial bias statistics with respect to all surface observations and by hemisphere for each initial condition treatment."

Page 10 L. 18-20: The sentence starting with 'However, because…' is hard to follow and should be edited.

We have broken this into two sentences to improve flow and clarity: "However, our a priori flux and lifetime are broadly consistent with independent observational constraints (Prather et al., 2012), whereas an annual N_2O source of 20+ Tg N would yield a higher-than-observed atmospheric growth rate. A biased initial mass field is thus the more tenable explanation for the negative model:measurement residual trend."

Page 11 L. 29: '…implying that the global annual a priori flux is too high.' How does this square with the arguments presented that some sources are underestimated in bottom-up approaches? Please clarify.

We did not mean to imply that an underestimate of certain sources necessarily leads to an underestimate in the global source. We have added a clarification here as follows: "the global annual a priori flux (from all sources combined)".

Page 12 L. 17-18: It would be helpful to indicate the regions in Figure 7 where authors feel most confident of results and then discuss only these regions in detail.

Thank you for the suggestion, but we wish to retain comparisons to other studies for each region and feel the separate sections helps the reader quickly find results for a region of interest. For regions where the results are more uncertain due to low observational constraints we mention this explicitly in the corresponding section.

L. 27: Please refer to Fig. 3 after 'Both the standard and SVD-based inversions call for a large increase (2-3×) in emissions from the US corn belt…' Here and in the discussion that follows in is sometimes difficult to compare the a priori and a posteriori results. Perhaps plotting the difference (increase or decrease in comparison to the a priori map would help the reader to follow the presentation?

Thank you for the suggestion. We have now included a reference to Fig. 3 after that phrase in the text. We have also added maps of the a posteriori emission increment (a posteriori – a priori) in Fig. 3 to aid the reader in identifying areas of increase/decrease relative to the prior.

L. 30: I do not follow why the authors single out 'underrepresentation of the indirect N2O source associated with leaching and runoff from agricultural soils' as the likely reason for magnitude of upwards adjustment derived in this study. As suggested in the comments for introduction there are other factors that could be having an impact.

The indirect source is the one most supported in the literature for this region, but other sources certainly could be contributing to the underestimate here. We have now added a mention of the potential impact of freeze-thaw and direct emissions here, as well as later in the conclusions.

Page 13 L. 1-2: Overestimation of natural emissions is used to explain the downward adjustment for western US and Canada. Could there possibly be other reasons? Gerber et al. 2016 show smaller fertilizer emission factors for these regions than usually used in inventories and this should also be considered here. A comparison with Gerber et al. for the other regions should also be made (similar results seen for increases in emissions in southern China).

Yes, it is certainly possible that direct agricultural emissions also contribute to the overestimate in western US and Canada. We have added a reference to Gerber et al. (2016) at the end of Section 4.3.1 to note the lower emission factors they found here. We also added a reference in Section 4.3.5 to support a potential underestimate of direct emissions in China when assuming a linear emission factor.

Page 15 L. 13-14: Can authors really state the reason for disagreement? Please see comment above. Is it possible that regions in western US and Canada have lower N2O emissions than the a priori model predicts due to lower fertilizer use and/or drier conditions (less use of irrigation?).

See our reply to the previous comment. We also clarify at the end that the underestimate from fertilized agricultural soils is specific to the US corn belt and possibly Asia where N input exceed crop demands.

L. 18-19: I am not sure why 'Seasonality in our prior emissions is dominated by the natural soil source.' Wouldn't fertilizer related emissions also be seasonal?

Yes, but the EDGARv4.2 emissions used here are annual so do not have any seasonality in the a priori emissions. We have added a reminder of this at the beginning of this sentence to clarify.

L. 24: 'November-December peak, and a May-June minimum': this is difficult to see in the figure. Perhaps are more detailed X-axis labels would help.

We have updated the x-axis here to be consistent with the updates made to Fig. 2: added 4/10 to the left-hand side of the axis, and slightly increased the interval of the axis labels.

L. 25: Fix 'an a'.

Thanks for catching this. We have fixed the error

L. 30; No need to use abbreviation (STE) as only used once.

We now spell out 'stratospheric-troposphere exchange' in place of the STE abbreviation here.

Page 16 L. 5-6: It is possible that indirect emissions are the reason for discrepancies between measurements and model. Would this also be the case for other regions where the same model for the a priori emissions is used? Could the differences be due to freeze/thaw emissions or higher than expected direct N2O emissions due to high N application rates (in exponential part of non-linear curve), which are not considered in the a priori emissions? Also, I am a bit confused by 'the fact that it is also one of the only sites located in an agricultural source region…' Could such discrepancy only show up in places where measurements are done at an agricultural site? Are other agricultural source regions being missed because there are no monitoring sites close by?

Here we simply meant to highlight the negative model-measurement bias at this site (as it is unique from other surface sites used in the inversion), and note that the sign of the bias here is consistent with earlier studies that link it to an underestimate of indirect emissions. The site is situated on drained lands, so the result may not be representative of other agricultural systems. We have rephrased as follows: "…inversion period. Located in an agricultural region composed mainly of drained lands, the low model bias is consistent with previous findings…"

L. 11-12: '…with the North American results exhibiting separate spring and summer peaks (plus a fall-winter enhancement in the SVD-based inversion)': I had difficulty seeing this in the figure. Perhaps better X-axis labels would help here as well.

We have now included x and y-axis labels on all panels in Fig. 7 to help the reader more quickly see when the peaks are occurring. The SVD-based peak referred to in the text occurs in October, so we now mention this explicitly in the text.

Page 16 L. 28-29: '…which have been shown (Chen et al., 2016) to peak earlier (indirect emissions) and later (direct emissions) in the growing season': I am confused as to why the indirect emissions would peak earlier since they derive from N that is lost from the fertilizer application and the nitrified or denitrified in water ways (after leaching or run-off) and soils (after dry deposition). The earlier peak seems more consistent with emissions due to spring thaw. Conclusions: comments made above apply here as well.

We note here that based on the IPCC definition: "Indirect pathways involve nitrogen that is removed from agricultural soils and animal waste management systems via volatilization, leaching, runoff, or harvest of crop biomass", so there is not an indication of seasonality here. Indirect emissions in the US Corn Belt are high in April-June when tile drainage and stream discharge peak. However, the reviewer is correct that spring thaw is also a possible contributor, and we have edited the text to reflect this. Additionally, many farmers in the US Corn Belt apply fertilizer in the fall, which would serve as a source of nitrogen to be released in the spring. As such, we have added the following sentence to the end of this section: "Fall fertilizer application is also common in the US Corn Belt—more than one third of corn farmers in Minnesota do their main N application during this time (Beirman et al., 2012)—which could explain the October peak in the SVD-based results, and provide a source of nitrogen that would be released in the early spring thaw and subsequent runoff period." We also note in Section 4.3.1 the following: "However, other processes could also contribute, such as freeze-thaw emissions or direct emissions after spring fertilizer application. The timing of these processes, and that of peak stream flow, correspond to the dominant modes of ambient N_2O variability observed in this region (Griffis et al., 2017)."

Table 1: explain which sites are 'remote'.

We have added a list of the remote sites as a footnote to the table.

Table 2: spell out SH, NH in heading

We have now spelled out Northern Hemisphere, Southern Hemisphere in the heading and caption of the table.

Figure 2: Give time period (April 2010 to…) in caption and add 4/10 to X-axis labels. Use of letters in a more frequent interval may help the reader find peaks/lows discussed in text.

Thank you for the suggestion. We have added the time period (April 2010 to April 2012) to the caption, added 4/10 to the left-hand side of the axis, and slightly increased the interval of the axis labels

Fig. 3: some pixels appear black on maps. Is that correct? It would be helpful to plot difference between two approaches instead of absolute amount so that areas of discrepancy can be identified more easily.

There are no black pixels in the emission maps in Fig. 3—perhaps this is just how the darkest red color appears in print? We have now added maps of the a posteriori emission increment (a posteriori – a priori) in Fig. 3 to aid the reader in identifying areas of increase/decrease relative to the prior.

Response to anonymous referee #2

This paper uses a multi-inversion hierarchy to derive top-down constraints on N2O emissions for 2011. The goal is to make a detailed evaluation of the 3 different methods and their impacts on inversion results. All methods are based on the adjoint of the GEOS-Chem chemical transport model, where 4D Var is considered the "standard" approach, as well as two alternative ways for aggregating the results, given that the existing observational network is insufficient to fully constrain N_2O emissions at the gridscale level. The first approach uses the 4DVar method, but aggregated to the traditional 6 continents and 3 oceans. The more novel approach tested is the new SVD-based technique based on the "prior- preconditioned Hessian of the 4D-Var cost function." An additional goal is to address the impact of initial condition uncertainties using 6 different approaches. This analysis is performed first and an optimal approach is selected for use in the evaluation of the 3 different inversion methods.

The paper is well written and logically organized. While some of the mathematics, particularly the SVD approach, are beyond my ability to evaluate, I found the results and discussion interesting and insightful. My main criticisms are, first, there seems to be a predisposition to claim the SVD results as the "best estimate of the true global flux." This conclusion is not clearly based on objective criteria. Other interpretations that might be more critical of SVD are not discussed, including the odd, spiky SVD results (e.g., in South America, Africa and the Tropical Oceans in Figure 7). Second, there is an unwarranted emphasis on the results of Chen et al. 2016, which are often presented as though they were primary results of the current study (see further comments below). However, these are minor criticisms of what is overall an impressive and interesting body of work. I recommend publication with some relatively minor revisions detailed below.

We wish to thank the reviewer for their positive evaluation of our manuscript. Please find our responses to specific comments below, where the comment is in italics and our response is in bold.

Abstract L31-32 "the inversions reveal a major emission underestimate in the US Corn Belt (which may extend to other regions), likely from underrepresentation of indirect N2O emissions from leaching and runoff. Please clarify an underestimate relative to what? Also, the last part of this sentence is supported

only on p12L30 with a reference to Chen et al. 2016. It is not supported by the current study and does not really belong in the abstract as a primary new finding.

We have deleted the reference to leaching and runoff here, and clarified that the underestimate is in the prior bottom-up inventory used.

As an aside, I will make a few comments about Chen et al. 2016, which is referenced multiple times (e.g., again on P17L27) as the source of the conclusion that the underestimate of indirect emissions is responsible for the underestimate of agricultural emissions in prior inventories. Realistically, I don't think the Chen et al. methodology is able to separate indirect and direct emissions. Their prior direct agricultural source is based on EDGAR, which is at least somewhat reliable since it is computed using gridded N inputs from fertilizer, etc. multiplied by emission coefficients. In contrast, the indirect source is based on the CLM45-BGC nitrate leaching and runoff flux, which is unreliable and almost certainly wrong (see, e.g., Houlton et al., Nature Climate Change, 5, 398, 2015). The Chen methodology then assumes those 2 prior sources accurately represent the spatial and temporal distribution of direct and indirect N2O emissions, respectively. That methodology is fraught with uncertainty. Moreover, the fact that (as stated on p16L28) indirect emissions peak earlier than direct emissions is a red flag that something is wrong. This result doesn't make sense, given that indirect emissions, by IPCC definition, occur later and downstream/downwind of direct emissions.

We would like to clarify a few points in the above comments on the Chen et al. (2016) paper. First, the Houlton et al. (2015) paper cited by the reviewer used the CLM-CN coupled model, which has a different solution for nitrate leaching and runoff than the CLM45-BGC model used in the Chen et al. (2016) paper. Second, the Chen et al. (2016) methodology does not assume the temporal distribution of a priori emissions is correct, as they solve for monthly fluxes. Third, a more recent paper (Griffis et al., PNAS, 2017), obtains very similar seasonality using different a priori emissions, which supports the Chen findings. However, Chen et al. (2016) is not being reviewed here and so we focus the rest of our response on issues relevant to our manuscript.

Based on the IPCC definition: "Indirect pathways involve nitrogen that is removed from agricultural soils and animal waste management systems via volatilization, leaching, runoff, or harvest of crop biomass", so there is not an indication of seasonality here. Indirect emissions in

the US Corn Belt are high in April-June when tile drainage and stream discharge peak. Additionally, many farmers in the US Corn Belt apply fertilizer in the fall, which would serve as a source of nitrogen to be released in the spring. As such, we have added the following sentence to the end of this section: "Fall fertilizer application is also common in the US Corn Belt—more than one third of corn farmers in Minnesota do their main N application during this time (Beirman et al., 2012)—which could explain the October peak in the SVD-based results, and provide a source of nitrogen that would be released in the early spring thaw and subsequent runoff period." We also added the following sentences in Section 4.3.1 to indicate that different processes (beyond just leaching and runoff) could be driving the overall underestimate of emissions in this region: "However, other processes could also contribute, such as freeze-thaw emissions or direct emissions after spring fertilizer application. The timing of these processes, and that of peak stream flow, correspond to the dominant modes of ambient N_2O variability observed in this region (Griffis et al., 2017)."

P2L24 Crutzen et al., 2008; Davidson, 2009 are not really bottom-up emissions. They are based more on a top-down approach (in a global box model sense) of comparing the observed atmospheric N2O increase to the rate of external N inputs and anthropogenic N fixation.

Thank you for the clarification. We have deleted the term "Bottom-up" from the beginning of this sentence.

P3L10-12 It seems somewhat overcritical to say previous aggregation has been informal and ad hoc. It's been based largely on geographical and political boundaries, i.e. North vs. South America, Pacific vs. Atlantic Ocean, etc., which are logical regions of interest.

Good point. We have replaced the phrase "in an informal ad-hoc way" to "based on physical or political boundaries".

P3L10-18 Exact totals are given for the ocean, GFED and EDGAR non-agricultural sources, but the Saikawa non-agricultural source and the EDGAR agricultural source are not specifically stated, yet these are the largest component sources. Please report them too. Two additional points are that the Saikawa source was based on a global model without cropland, such that it included a "non-agricultural" soil source from land such as the US Midwest where crops are grown. Also, the

EDGARv4.2 total is about 1.7 TgN/yr from industry, waste water and energy. To bring up the reported 2.3 TgN/yr, I wonder if the authors have included the EDGAR savanna, forest, grass, and agricultural fire fluxes (of 0.84 Tg N/yr), which might be redundant with the GFED source? (Note: my numbers are from 2005 and thus may be slightly different from 2008.)

Thank you for catching this. We did not include the EDGAR fire sources in our 2.3 Tg N yr^{-1}, but accidentally included indirect emission from NO_x and NH_3 deposition (~0.4 Tg N) and manure management (~0.2 Tg N) in this total rather than in the reported agricultural source total. Thus, the EDGARv4.2 total for 2008 is about 1.7 Tg N yr^{-1} as you noted. We now report specific totals for the Saikawa source (7.5 Tg N) and EDGAR agricultural soil direct+indirect (3.5 Tg N yr^{-1}) and manure management sources separately.

P4L29 Please state the time resolution of the inversion somewhere around here.

We have added "monthly" to the first line of this paragraph.

P5L19 Negative emission scaling factors may be appropriate for some oceanic regions, especially during seasonal cooling in regions where the biological source is small and thermal solubility-driven uptake may dominate the air-sea flux.

We do have negative fluxes where uptake dominates the air-sea flux in our a priori oceanic emissions. Our inversion approach does not require positive fluxes, but it does assume that the sign of the a priori flux is correct in each grid square. We now mention this explicitly in the text here.

P5L27-29 Can we infer from this that the total observational uncertainty (which is also referred to as model-data mismatch uncertainty) is typically about 0.45 ppb? It would be useful to state this. It is interesting and unexpected that the observational uncertainty dominates the model representation uncertainty. At only 0.2 ppb, the model representation error seems substantially underestimated. Also, considering that the grid resolution is 4x5 degrees, how many grid boxes actually "surround" any given observation and what kind of heterogeneity is missed inside the actual box that contains the measurement?

Correct, this would correspond to a mean observational error of ~0.45 ppb, which we now mention in the text. We also note that values extend up to ~4 ppb. Given the coarse horizontal

resolution, we could be underestimating the representation error for near-source observations. However, we have since run a test standard inversion with tripled observational error and get very similar results (global flux of 17.8 Tg N).

P7 The SVD-method is complex to the point of being unfathomable for many readers (including me!), so we must take it on faith that the calculation is accurate. Given the lengthy form of equation 5, I am concerned that it would be easy for human errors to slip into the calculation. What assurances do we have that such errors will be detected?

Three of the co-authors have rechecked the equations for accuracy, and no errors have been detected.

P9-10 I found this section difficult to follow and did not emerge with a clear understanding of why certain initialization methods are better than others. I'm not sure what to suggest to help clarify, but one step might be to include some columns for the NH-SH gradient in Table 2 in addition to (or perhaps instead of) the separate NH and SH bias columns. Those are not really referred to in the text, while the "overly strong interhemispheric gradient" is mentioned on P9L26 but is not obvious in Table 2.

We have tried to clarify here that an overly strong interhemispheric gradient is indicated by the fact that the model has a high bias in the Northern Hemisphere and a low bias in the Southern Hemisphere. We have also removed the subsequent reference to the interhemispheric gradient and replaced it with the following sentence: "The interpolation methods without subsequent spinup (AprZonal, AprKriging) perform better in terms of initial model:measurement bias – in the global mean and in each individual hemisphere."

P11L18 The statement that SVD "appears to provide the best estimate of the true global flux" seems based on fairly limited and/or subjective criteria. Furthermore, it is not obviously true that SVD agrees best with HIPPO. In fact, it seems to agree worst from 30S-30N. (This is attributed on P11 to the fact that "the spatial distribution (in the tropics) is particularly difficult to resolve," but this is not necessarily a satisfactory explanation.) Is the comparison to HIPPO based on subjective visual inspection or some more quantitative measure? Also, are we sure the HIPPO calibration scale is not systematically biased from the data used in the inversion, especially given the adjustments described in section 2.3?

We have now deleted the claim that the SVD-based inversion provides the best estimate of the true global flux. We also outline more specifically where/when the agreement with HIPPO is improved. The sentence now reads: "It also gives a better comparison to HIPPO IV and V measurements in the southern extratropics and to HIPPO V in the northern extratropics (see below)." We have also edited the last two sentences of Section 4.1 to read "The lower global flux obtained with the SVD-based approach (Fig. 3 and Table 3) is thus the reason for this correction, implying that the global annual a priori flux (from all sources combined) may be too high. We note that a slight low bias does emerge in the tropics in the SVD-based approach, where observational constraints are low." We have also edited the language in the conclusions to be consistent with this. As for the calibration, we have adjusted the HIPPO QCLS data based on concurrent flask observations, which are on the NOAA scale. We now mention this at the end of Section 2.3.

P13 section 4.3.3 The results for Europe indicate a fairly dramatic reduction from the prior. Please state the total non-agricultural prior source in EDGARv4.2. How much of the total 1.70 Tg N prior does it comprise?

We had already included the contribution of EDGARv4.2 non-agricultural sources to the total in Europe (~40%) in Section 4.3.3. However, since we accidentally lumped manure management and indirect emissions from NO_x and NH_3 deposition in that total, we have revised this number. The total European non-agricultural source in EDGARv4.2 is about 0.5 Tg N, which is about 30% of the total prior emissions here. The resulting relative a posteriori adjustments for soil and non-agricultural sources, when integrated over Europe, are thus comparable in magnitude, and we have edited the text to reflect that.

P14L31 The results of 3.35-3.48 are above the range found by Buitenhuis (2.4 +/- 0.8).

Correct, we already note at the end of this sentence that our optimized oceanic fluxes are higher than that found by Buitenhuis. However, they are closer to that estimate than the results of Thompson et al. (2014), which is what we meant by "more consistent with". We have now clarified this in the text.

P17L20 It's perhaps notable here that the EDGAR industrial source has dropped by about a factor of 2 in version subsequent to v4.2 used here.

Thank you for mentioning this. We have added a note mentioning this at the end of this bullet point in the text.

P17L23-24 I think the main issue here is that the seasonality in the existing inventories used here is governed by natural soil emissions from a model without crops. The EDGAR agricultural source with no seasonality is then added. However, the hotspot of emission is in agricultural areas where the seasonality is influenced by spring fertilizer input. Thus the seasonality of existing inventories is predictably wrong from the outset.

The reviewer is correct that we should expect some degree of seasonal bias given that annual EDGAR fluxes were used a priori. We have now deleted the phrase "than our current inventories suggest" from this sentence, and emphasize that the optimized seasonality is consistent with other studies.

P31 Figure 3 caption. Do the bars show the median (as currently stated) or the mean of the 3 inversions? How meaningful is the median of just 3 values? Would it be better to just show all 3 results + prior, i.e. 4 bars per region?

The bars do show the median of the a posteriori values as stated—the median was chosen so it is easy to infer all three values (min, median, and max) from the figure. We previously tried plotting 4 bars per region but found the plot too busy, so prefer to keep the two bars per region, but we have thickened the a posteriori error bars to more easily see the range.

P34. I'm not sure Figure 6 adds much value to the paper. Furthermore, why is the KCMP measurement of primary interest to the current study?

KCMP is of primary interest to our study given that i) it is the only site with a near-persistent model underestimate, ii) it is in an agricultural region comprised of drained lands (now mentioned at the end of Section 4.4.1), and iii) the emission processes for this ecosystem type are not well represented in current emission inventories, and have been linked to underestimated indirect N_2O emissions associated with leaching and runoff. As for the value of Fig. 6, we find it

helpful to show the seasonal model biases in N_2O mixing ratio that exist before showing the a priori and a posteriori seasonal fluxes in Fig. 7.

Authors' changes in the manuscript are below, with changes tracked

Top-down constraints on global N_2O emissions at optimal resolution: application of a new dimension reduction technique

Kelley C. Wells[1], Dylan B. Millet[1], Nicolas Bousserez[2], Daven K. Henze[2], Timothy J. Griffis[1], Sreelekha Chaliyakunnel[1], Edward J. Dlugokencky[3], Eri Saikawa[4], Gao Xiang[5], Ronald G. Prinn[6], Simon O'Doherty[7], Dickon Young[7], Ray F. Weiss[8], Geoff S. Dutton[3,9], James W. Elkins[3], Paul B. Krummel[10], Ray Langenfelds[10], and L. Paul Steele[10]

[1]Department of Soil, Water, and Climate, University of Minnesota, St. Paul, Minnesota, USA
[2]Department of Mechanical Engineering, University of Colorado at Boulder, Boulder, Colorado, USA
[3]Earth System Research Laboratory, NOAA, Boulder, Colorado, USA
[4]Department of Environmental Sciences, Emory University, Atlanta, Georgia, USA
[5]Joint Program on the Science and Policy of Global Change, Massachusetts Institute of Technology, Cambridge, Massachusetts, USA
[6]Center for Global Change Science, Massachusetts Institute of Technology, Cambridge, Massachusetts, USA
[7]School of Chemistry, University of Bristol, Bristol, UK
[8]Scripps Institute of Oceanography, University of California San Diego, La Jolla, California, USA
[9]CIRES, University of Colorado at Boulder, Boulder, Colorado, USA
[10]Climate Science Centre, CSIRO Oceans and Atmosphere, Aspendale, Victoria, Australia

Correspondence to: Dylan B. Millet (dbm@umn.edu)

Abstract. We present top-down constraints on global~~,~~ monthly N_2O emissions for 2011 from a multi-inversion approach and an ensemble of surface observations. The inversions employ the GEOS-Chem adjoint and an array of aggregation strategies to test how well current observations can constrain the spatial distribution of global N_2O emissions. The strategies include: (1) a standard 4D-Var inversion at native model resolution (4° × 5°), (2) an inversion for six continental and three ocean regions, and (3) a fast 4D-Var inversion based on a novel dimension reduction technique employing randomized singular value decomposition (SVD). The optimized global flux ranges from 15.9 Tg N yr^{-1} (SVD-based inversion) to 17.5-17.7 Tg N yr^{-1} (continental-scale, standard 4D-Var inversions), with the former better capturing the extratropical N_2O background measured during the HIAPER Pole-to-Pole Observations (HIPPO) airborne campaigns. We find that the tropics provide a greater contribution to the global N_2O flux than is predicted by the prior bottom-up inventories, likely due to underestimated agricultural and oceanic emissions. We infer an overestimate of natural soil emissions in the extratropics, and find that predicted emissions are seasonally biased in northern midlatitudes. Here, optimized fluxes exhibit a springtime ~~versus summertime~~ peak ~~more~~ consistent with the timing of spring fertilizer and manure application, soil thawing, and elevated soil moisture. Finally, the inversions reveal a major emission underestimate in the US Corn Belt ~~(which may extend to other intensive agricultural regions), likely from underrepresentation of indirect N_2O emissions from leaching and runoff~~in the bottom-up inventory used here. We extensively test the impact of initial conditions on the analysis and recommend formally

optimizing the initial N_2O distribution to avoid ~~aliasing~~ biasing the inferred fluxes. We find that the SVD-based approach provides a powerful framework for deriving emission information from N_2O observations: by defining the optimal resolution of the solution~~state vector~~ based on the information content of the inversion, it provides ~~useful~~ spatial information that is lost when aggregating to political or geographic ~~ad hoc~~ regions, while also provding more ~~better resolving~~ temporal ~~features~~ information than a standard 4D-Var inversion.

1 Introduction

Nitrous oxide (N_2O) is a long-lived greenhouse gas (τ ~122-131 years; Volk et al., 1997; Prather et al., 2012) with substantial impacts on both climate and stratospheric chemistry. It has a global warming potential far exceeding that of CO_2 (265× on a 100-year timescale; Myhre et al., 2013), and its emissions weighted by ozone depletion potential currently exceed those of all other substances (Ravishankara et al., 2009). The global N_2O source is reasonably well constrained (15.7 to 20.1 Tg N yr^{-1} for years 1999-2009; Prather et al., 2012; Saikawa et al., 2014; Thompson et al., 2014a; Thompson et al., 2014c) by its atmospheric abundance and estimated lifetime. However, attribution of ~~the~~ this source to specific regions and sectors ~~is~~ has been hindered by the sparse global observing network and by the ~~strong spatio-temporal variability in N_2O emissions combined with~~ weak variability in ~~atmospheric~~ N_2O mixing ratios ~~and a sparse global observing network~~ (e.g., Wells et al., 2015). Quantitative interpretation of atmospheric N_2O measurements in terms of globally resolved emissions thus first requires a rigorous assessment of how results hinge on the modeling framework employed. Here, we apply a hierarchy of model resolutions, including a new method that formally defines the state vector for optimization based on the information content of the observations, in a global inverse modeling framework to address this need. We use this model hierarchy with a global suite of observations to:~~-~~ i) quantify the spatial and seasonal distribution of N_2O emissions for 2011, ii) examine what features of these results are robust across model configurations, and iii) assess the implications for current understanding of the N_2O budget and future research needs.

The primary sources of atmospheric N_2O are microbial denitrification and nitrification, which lead to N_2O production in soils (Firestone and Davidson, 1989), ocean waters (Elkins et al., 1978; Cohen and Gordon, 1979), and in streams, rivers, and lakes (Seitzinger and Kroeze, 1998; Beaulieu et al., 2011). Global mean N_2O mixing ratios rose by 0.85 ± 0.1 ppb yr^{-1} from 2001-2015 (based on NOAA surface measurements) primarily due to increased use of ~~nitrogen-based~~inorganic fertilizers and manure (Galloway et al., 2008; Davidson, 2009; Park et al., 2012) and the nonlinear response of N_2O emissions to ~~fertilizer application~~N inputs in some agricultural systems (Shcherbak et al., 2014). ~~Bottom-up e~~Estimates for the global agricultural flux range from 4.3-6.3 Tg N yr^{-1} (Mosier et al., 1998; Crutzen et al., 2008; Davidson, 2009)~~:~~, ~~which~~ this includes emissions occurring on-field (i.e. 'direct' emissions from fertilized ~~crops~~fields), downstream (~~so-called~~ 'indirect' emissions from N leaching and runoff, and from deposition of volatilized NO_x and NH_x), and from manure management. ~~However~~These sources are all subject to large uncertainties~~., a body of~~ For example, by assuming a linear flux response to fertilizer application, one can either under- or overestimate emissions depending on the application rate

Formatted: Subscript

Formatted: Subscript

Formatted: Subscript

Formatted: Subscript

(Shcherbak et al., 2014; Gerber et al., 2016). R~~r~~ecent work also suggests that the indirect N_2O ~~emissions downstream from the site of fertilizer application~~flux could be 2.6-9 times larger than is presently accounted for in bottom-up estimates (Griffis et al., 2013; Turner et al., 2015), which would imply an underestimate of the ~~importance of~~ agricultural ~~sources for~~contribution to the overall N_2O budget. Non-agricultural soils and oceans are thought to contribute an additional 7.4-11 Tg N yr^{-1} (Saikawa et al., 2013) and 1.2-6.8 Tg N yr^{-1} (Nevison et al., 1995; Jin and Gruber, 2003; Manizza et al., 2012), respectively, to the global N_2O source. Industrial, transportation, and biomass burning emissions also exist but are thought to be relatively minor, totaling 1.2-1.8 Tg N yr^{-1} (Prather et al., 2001).

Because microbial nitrification and denitrification, and the subsequent soil-atmosphere N_2O flux, ~~in soils~~ depend strongly on factors such as soil moisture, temperature, ~~soil type, and fertilizer application timing~~physical characteristics, and N availability (e.g., Potter et al., 1996; Bouwman, 1998; Kim et al., 2012; Bouwman et al., 2013; Butterbach-Bahl et al., 2013; Griffis et al., 2017), N_2O emissions can exhibit major temporal and spatial variability. For example, Wagner-Riddle et al. (2017) ~~estimated~~ found that short-duration freeze-thaw cycles can account for 35-65% of the ~~total~~ annual direct N_2O emissions from seasonally frozen croplands ~~globally~~, and that neglecting this contribution would lead to a 17-28% underestimate of the global N_2O source (direct+indirect) from agricultural soils. This type of variability poses a major challenge to bottom-up and top-down efforts to quantify N_2O surface fluxes and attribute them to specific times, locations, and mechanisms. The relatively sparse coverage of measurement sites and low atmospheric variability (because of the long N_2O lifetime, surface mixing ratios typically vary by < 10 ppb ~~due to the long N_2O lifetime~~on a ~325 ppb background) compound the challenge, and limit the spatial and temporal resolution at which emission fluxes can be inferred (Wells et al., 2015). As a result, global N_2O inversions often employ some aggregation strategy to optimize emissions for a small set of geographic regions (e.g., Hirsch et al., 2006; Huang et al., 2008; Saikawa et al., 2014). However, in the past this aggregation ~~is typically~~has been done ~~in an informal, ad-hoc way~~based on physical or political boundaries rather than by formally determining the degrees of freedom (DOFs) in the inverse system – which leads to aggregation errors and sub-optimal results. Work on CO_2 inversions has also highlighted this issue (e.g., Kaminski et al., 2001) and the resulting importance of determining the proper state vector size for optimal results (Bocquet et al., 2011).

Another key challenge is that because of the long N_2O lifetime, inaccuracies in model initial conditions can lead to large biases in the subsequent optimized emissions (Thompson et al., 2014c). Past global N_2O inversion studies have established the initial conditions in a variety of ways: from a forward model spin-up that is then evaluated against observations (e.g., Huang et al., 2008); by including the initial condition as a separate adjustable parameter in the source optimization (e.g., Saikawa et al., 2014; Thompson et al., 2014a); or from interpolation of atmospheric observations (e.g., Wells et al., 2015). To our knowledge there has not yet been a detailed evaluation of these different methods and their impacts on N_2O source inversions. Such information is needed to establish the degree to which uncertainties in the initial conditions can propagate to errors in the optimized N_2O emission estimates.

In this paper, we address the above uncertainties in a quantitative way using a multi-inversion hierarchy to derive top-down constraints on N_2O emissions for 2011. We use the adjoint of the GEOS-Chem chemical transport model (CTM) to solve for

Formatted: Subscript

Formatted: Subscript

Formatted: Subscript

monthly fluxes at the model grid box scale as well as at geographically aggregated continental scales. We compare these results with those obtained using a new dimension reduction technique based on the SVD of the so-called prior-preconditioned Hessian of the 4D-Var cost function (Bousserez and Henze, 2017). This new SVD-based approach allows us to solve for fluxes at optimal spatiotemporal ~~scales~~resolution, as defined by the information content of the N_2O observations – thus maximizing the DOFs for the inversion and avoiding any need for spatial aggregation based on geography or source type. It also offers significant time savings over standard grid-based 4D-Var approaches, due to the use of efficient randomized SVD algorithms (Halko et al., 2011). The initial conditions for the above inversions are constructed in a variety of ways, and we use observations and model simulations to assess their accuracy and associated impacts on optimized N_2O fluxes. We then evaluate these optimized emissions using independent airborne measurements and interpret the results in terms of underlying emission processes, with specific emphasis on the role of model resolution in affecting the solution, and on those features that appear most robust (and most uncertain) across model configurations.

2 Methods

2.1 GEOS-Chem N_2O simulation

The N_2O simulation employed here, previously described by Wells et al. (2015), is based on the GEOS-Chem CTM (www.geos-chem.org) with GEOS-5 assimilated meteorological data from the NASA Goddard Earth Observing System. We use a horizontal resolution of 4° × 5° with 47 vertical levels from the surface to 0.01 hPa, and time steps of 30 minutes for transport and 60 minutes for emissions and chemistry. The simulation period spans April 2010-April 2012 (the start date is selected to match the initiation of N_2O measurements at the KCMP tall tower site discussed later).

A priori N_2O emissions for anthropogenic, non-agricultural sources (including industrial processes, transportation, residential, and wastewater emissions) are from the Emission Database for Global Atmospheric Research (EDGARv4.2; http://edgar.jrc.ed.europa.eu), which are provided annually and total 1.7~~2.3~~ Tg N yr^{-1} for 2008. Monthly N_2O emissions from non-agricultural soils are from CLMCN-N_2O as described by Saikawa et al. (2013), and total 7.5 Tg N yr^{-1} for 2011. These emissions have been shown to accurately capture the magnitude and seasonality of soil emissions in the Amazon, but exhibited less skill in reproducing the observed seasonal cycle in northern midlatitudes (based on data from New Hampshire; Saikawa et al., 2013). The magnitude of these emissions varies depending on the meteorological forcing dataset used; forcings used here are from the MIT Integrated Global System Model (IGSM) fully coupled transient 20th century climate integration (Sokolov et al., 2009). ~~Together with the~~ Adding these to the annual EDGARv4.2 direct and indirect (leaching and runoff) agricultural emissions (3.5 Tg N yr^{-1}), indirect emissions from NO_x and NH_3 deposition (0.4 Tg N yr^{-1}), and emissions from manure management (0.2 Tg N yr^{-1}), ~~this~~ leads to an a priori global soil N_2O source of 11.6~~0~~ Tg N yr^{-1} for 2011. Biomass burning emissions are computed monthly based on the Global Fire Emissions Database version 3 (GFED3; van der Werf et al., 2010), totaling 0.6 Tg N yr^{-1}, while monthly oceanic N_2O emissions are from Jin and Gruber (2003) and total 3.5 Tg N yr^{-1}. The global annual a priori N_2O flux for 2011 is then 17.4 Tg N yr^{-1}, in the range of recent top-down

Formatted: Subscript
Formatted: Superscript
Formatted: Superscript
Formatted: Subscript
Formatted: Subscript
Formatted: Superscript

estimates (16.1 to 18.7 Tg N yr^{-1} for years 2006-2008; Saikawa et al., 2014; Thompson et al., 2014c). Stratospheric loss of N_2O via photolysis and reaction with $O(^1D)$ is calculated from 3-D loss frequencies archived monthly from Global Modeling Initiative (GMI) simulations driven by MERRA meteorological fields; the resulting N_2O lifetime is ~127 years (note that the value depends on the initial spatial distribution of N_2O in the model).

The long N_2O lifetime necessitates accurate characterization of initial conditions to avoid biasing the optimized fluxes (e.g., Thompson et al., 2014c). In our work, we construct six sets of initial conditions from global N_2O observations and evaluate the corresponding impacts on the inferred fluxes. Initial condition fields are constructed based on either data interpolation or 4D-Var optimization, with details discussed in Section 3.

2.2 Inversion frameworks

We employ three inversion methods with varying resolution to solve for monthly N_2O emissions over two years (April 2010 – April 2012) based on global surface observations. The first of these is a 4-D Var inversion that iteratively optimizes emissions on the native model grid (here 4° × 5°) using gradients computed with the GEOS-Chem adjoint model. This has the advantage of avoiding any aggregation errors associated with traditional clustering methods. However, our previous work (Wells et al., 2015) has shown that the degrees of freedom for atmospheric N_2O inversions is typically much less than the native model grid dimension, and furthermore that native resolution optimizations have limited ability to resolve any temporal (e.g., seasonal) N_2O emission biases. We therefore apply two alternate approaches to reduce the dimension of the inverse problem: 1) a 4D-Var inversion solving for emissions on aggregated, geographically-defined land and ocean regions, and 2) a 4D-Var inversion solving for emissions on a reduced emission basis set defined using an SVD-based information content analysis. In all three frameworks we consider two emission sectors (terrestrial and oceanic), and optimize monthly fluxes. We present details for each of the three frameworks in the following sections.

2.2.1 Standard 4D-Var inversion

Our standard inversion is a 4D-Var optimization in which the state vector contains scaling factors for monthly N_2O emissions at 4° × 5°. The optimal set of emission scaling factors is obtained by minimizing the cost function, $J(\boldsymbol{x})$, which is a scalar containing contributions from the error-weighted model-measurement mismatch and the departure from the a priori values:

$$J(\boldsymbol{x}) = \frac{1}{2}\sum_{\boldsymbol{h}(\boldsymbol{x})\in\Omega}(\boldsymbol{h}(\boldsymbol{x})-\boldsymbol{y})^T\mathbf{S}_y^{-1}(\boldsymbol{h}(\boldsymbol{x})-\boldsymbol{y}) + \frac{1}{2}(\boldsymbol{x}-\boldsymbol{x}_a)^T\mathbf{S}_a^{-1}(\boldsymbol{x}-\boldsymbol{x}_a)\,, \quad (1)$$

where $\boldsymbol{x}$ is a vector of the parameters to be optimized (in this case, emission scaling factors), $\boldsymbol{x_a}$ contains the a priori values of those parameters, $\boldsymbol{y}$ is a set of observed N_2O mixing ratios, $\boldsymbol{h(x)}$ is a vector containing the simulated mixing ratios at the time and location of each observation, $\mathbf{S}_y$ and $\mathbf{S}_a$ are the observational and a priori error covariance matrices, and Ω represents the time-space domain of the observations.

We ~~find the cost function minimum by using~~use a quasi-Newton routine (Zhu et al.,1994; Byrd et al., 1995) to iteratively converge to min($J(\boldsymbol{x})$). At each iteration, we use the adjoint of GEOS-Chem to compute the gradient of $J(\boldsymbol{x})$ with respect to the emission scaling factor ~~using the adjoint of GEOS-Chem~~, and employ~~. We use~~ a lower bound of zero ~~to avoid negative emission scaling factors~~ and an upper bound of 10 based on our earlier work (Wells et al., 2015). This approach therefore implicitly assumes that the sign of the a priori flux (which can be negative over the ocean) is correct for each model grid square. The GEOS-Chem adjoint has previously been applied to a wide range of inverse problems for atmospheric composition, including constraining sources and sinks of long-lived greenhouse gases such as CO_2 (Deng et al., 2014; Liu et al., 2014; Deng et al., 2015, Liu et al., 2015), methane (Wecht et al., 2014; Turner et al., 2015), and N_2O (Wells et al., 2015), as well as aerosols and reactive trace gases (e.g., Henze et al., 2007; Kopacz et al., 2009; Wells et al., 2014).

A priori uncertainties are assumed to be 100% for both land and ocean emissions, with off-diagonal terms assuming correlation length scales of 500 and 1000 km, respectively, following prior work by Thompson et al. (2011; 2014a). Observational errors are calculated as the quadratic sum of measurement uncertainty (~0.4 ppb for most sites, see Section 2.4) and model transport uncertainty, with the latter estimated from the 3-D model variance in N_2O mixing ratios in the grid boxes surrounding any given observation (resulting in a mean uncertainty ~0.2 ppb at the surface). The corresponding mean observational uncertainty is ~0.45 ppb, with maximum values ~4 ppb. The solution presented here was calculated using 40 iterations, after which the cost function change per iteration is <1% and the total cost function reduction is ~65% (Fig. S2).

2.2.2 Continental-scale inversion

While the above approach avoids any aggregation error, the existing observational network provides insufficient information to constrain N_2O emissions in every 4° × 5° model grid square. Therefore, in an alternate inversion, we reduce the dimension of the inverse problem by solving for emission scaling factors on six continental (North America, South America, Europe, Africa, Asia, Oceania) and three ocean regions (northern oceans: 30° – 90° N, tropical oceans: 30° S – 30° N, and southern oceans: 30° – 90° S). Regions are mapped in Fig. S1 and are similar to those used in the TransCom N_2O model intercomparison study (Thompson et al., 2014b; 2014c), except with one rather than two Asian regions. While this inversion could readily be carried out analytically rather than numerically (owing to its small dimension) we instead use 4D-Var for consistency and to impose the same scaling factor bounds (0-10) as in the standard inversion. We thus use the GEOS-Chem adjoint to calculate the cost function gradient ($\nabla_{\boldsymbol{x}} J(\boldsymbol{x})$~~$\partial J/\partial \boldsymbol{x}$~~) aggregated over the 9 predefined regions. We then iteratively minimize $J(\boldsymbol{x})$, achieving a cost function change of < 1% per iteration (and total reduction of ~55%) after 28 iterations (Fig. S2).

2.2.3 SVD-based inversion

As an advance over standard aggregation methods such as the one described above, we also apply a new, efficient SVD-based information content analysis technique that maximizes the degrees of freedom of the inverse system while permitting us to solve for N_2O fluxes in a fast iterative framework. The method, based on synthesis and advancement of recent work~~s~~ in

this area (Flath et al., 2011; Bui-Thanh et al., 2012; Spantini et al., 2015) by Bousserez and Henze (2017), uses an optimal low-rank projection of the inverse problem that maximizes the observational constraints. Specifically, for a given dimension *k*, the optimal reduced space (Spantini et al., 2015; Bousserez and Henze, 2017) is spanned by the first *k* eigenvectors of the prior-preconditioned Hessian **G** (Flath et al., 2011):

$$\mathbf{G} \equiv \mathbf{S}_a^{\frac{1}{2}}\mathbf{H}^T\mathbf{S}_y^{-1}\mathbf{H}\mathbf{S}_a^{\frac{1}{2}} = \mathbf{V}\boldsymbol{\Lambda}\mathbf{V}^T, \quad (2)$$

where **H** is the tangent linear of the forward model, **V** is a matrix whose columns are the eigenvectors of **G**, and **Λ** is a diagonal matrix containing the eigenvalues of **G**. The following analytical approximation can then be used:

$$\mathbf{S}_{opt} = \mathbf{S}_a - \mathbf{S}_a^{\frac{1}{2}}\left(\sum_{i=1}^{k}\frac{\lambda_i}{\lambda_i+1}\boldsymbol{v}_i\boldsymbol{v}_i^T\right)\mathbf{S}_a^{\frac{1}{2}}, \quad (3)$$

where $\mathbf{S}_{\text{opt}}$ is the posterior error covariance matrix, while $\boldsymbol{v}_{i,i=1,..,k}$ and $\lambda_{i,i=1,..,k}$ are the eigenvectors and eigenvalues of **G**. This expression gives, in some sense, the lowest error rank-*k* approximation of $\mathbf{S}_{opt}$ (see Bousserez and Henze (2017) for details). The eigenvectors $\boldsymbol{v}_i$ can be interpreted as the most constrained modes in flux space, i.e. flux patterns that are independently constrained by the observations (Cui et al., 2014; Bousserez and Henze, 2017). These eigenvectors of the prior-preconditioned Hessian are efficiently calculated using a fully-parallelized randomized algorithm (Halko et al., 2011), as in Bui-Thanh et al. (2012) and Bousserez and Henze (2017). We use *k*=350 here, which employs nearly all modes with eigenvalues greater than 1.0 (Fig. S3), as modes with eigenvalues below this threshold are informed mainly by the prior.

From $\mathbf{S}_{opt}$ we can obtain the inversion averaging kernel, which gives a measure of how well emissions are constrained in a given location, as follows:

$$\mathbf{AK} = \mathbf{I} - \mathbf{S}_{opt}\mathbf{S}_a, \quad (4)$$

where **I** is the identity matrix and $\mathbf{S}_a$ is the a priori error covariance matrix. Optimized solutions in areas where the diagonal of **AK** is close to 1.0 are well-constrained by the observations. The trace of the averaging kernel gives the total degrees of freedom, i.e. the number of independent pieces of information that can be obtained in the inversion framework.

The posterior mean estimate of $\boldsymbol{x}$ can also be directly calculated from analytical formulas using the eigenvectors of **G** (Spantini et al., 2015; Bouserez and Henze, 2017). However, to impose a positivity constraint on the emissions, we rely here on the variational minimization framework as in the standard 4D-Var case. In order to leverage the use of the optimal basis set, we project both the cost function and its gradient onto the principal modes to obtain a reduced analytical formulation. The analytical expression for the reduced cost function (derivation presented in Appendix A) is:

$$J(\boldsymbol{x}) \approx \frac{1}{2}(\boldsymbol{x}-\boldsymbol{x}_a)^T\mathbf{S}_a^{-\frac{1}{2}}\sum_{i=1}^{k}\boldsymbol{v}_i\boldsymbol{v}_i^T\mathbf{S}_a^{-\frac{1}{2}}(\boldsymbol{x}-\boldsymbol{x}_a) + \frac{1}{2}(\boldsymbol{h}(\boldsymbol{x}_a)-\boldsymbol{y})^T\mathbf{S}_y^{-1}(\boldsymbol{h}(\boldsymbol{x}_a)-\boldsymbol{y}) + \frac{1}{2}(\boldsymbol{x}-\boldsymbol{x}_a)^T\mathbf{S}_a^{-\frac{1}{2}}\sum_{i=1}^{k}\lambda_i\boldsymbol{v}_i\boldsymbol{v}_i^T\mathbf{S}_a^{-\frac{1}{2}}(\boldsymbol{x}-\boldsymbol{x}_a) + \frac{1}{2}(\boldsymbol{h}(\boldsymbol{x}_a)-\boldsymbol{y})^T\mathbf{S}_y^{-\frac{1}{2}}\sum_{i=1}^{k}\lambda_i^{\frac{1}{2}}\boldsymbol{w}_i\boldsymbol{v}_i^T\mathbf{S}_a^{-\frac{1}{2}}(\boldsymbol{x}-\boldsymbol{x}_a) + \frac{1}{2}(\boldsymbol{x}-\boldsymbol{x}_a)^T\mathbf{S}_a^{-\frac{1}{2}}\sum_{i=1}^{k}\lambda_i^{\frac{1}{2}}\boldsymbol{v}_i\boldsymbol{w}_i^T\mathbf{S}_y^{-\frac{1}{2}}(\boldsymbol{h}(\boldsymbol{x}_a)-\boldsymbol{y}), \quad (5)$$

while the analytical approximation for the cost function gradient is:

$$\nabla J(\boldsymbol{x}) \approx \mathbf{S}_a^{-\frac{1}{2}}\sum_{i=1}^{k}\boldsymbol{v}_i\boldsymbol{v}_i^T\mathbf{S}_a^{-\frac{1}{2}}(\boldsymbol{x}-\boldsymbol{x}_a) + \mathbf{S}_a^{-\frac{1}{2}}\sum_{i=1}^{k}\lambda_i\boldsymbol{v}_i\boldsymbol{v}_i^T\mathbf{S}_a^{-\frac{1}{2}}(\boldsymbol{x}-\boldsymbol{x}_a) + \mathbf{S}_a^{-\frac{1}{2}}\sum_{i=1}^{k}\lambda_i^{\frac{1}{2}}\boldsymbol{v}_i\boldsymbol{w}_i^T\mathbf{S}_y^{-\frac{1}{2}}(\boldsymbol{h}(\boldsymbol{x}_a)-\boldsymbol{y}), \quad (6)$$

where k=350 is the number of modes retained in the approximation. Here, $\boldsymbol{h}(\boldsymbol{x}_a)$ are the model mixing ratios corresponding to the a priori emissions and $\boldsymbol{w}_i$ are the eigenvectors in observation space:

$$\boldsymbol{w}_i = \frac{1}{\sqrt{\lambda_i}} \mathbf{S}_y^{-\frac{1}{2}} \mathbf{H} \mathbf{S}_a^{\frac{1}{2}} \boldsymbol{v}_i. \quad (7)$$

Because the cost function and gradient depend only on the a priori model-measurement difference, the a priori and observational error covariances, and the eigenvectors of **G** (which are computed only once), this iterative inversion offers significant time savings, particularly for models with a low level of parallelization. Monthly N_2O emission scaling factors for the 2-year analysis window are derived in approximately 6 hours, versus over 100 hours for the standard and continental-scale inversions, and nearly all the computation time in the former case is spent on calculating the eigenvectors of **G**. The solution for the SVD-based inversion (with a projected cost function change of < 1% per iteration) is obtained after 60 iterations (Fig. S2). The full cost function reduction (calculated from a forward model run) is ~25% for this solution, whereas we achieve the minimum in the full cost function at a much earlier iteration (see Fig. S2). The divergence in the behavior of the projected and full cost function after this point may suggest that the weaker modes included here are not as well-approximated by the randomized SVD calculation as the dominant modes. An objective criteria for determining the error in the randomized SVD is the subject of a work in progress.

2.3 Atmospheric N_2O observations

Atmospheric N_2O observations used in our analysis include a global ensemble of surface measurements as well as airborne data from the HIAPER Pole-to-Pole Observations (HIPPO) campaigns (Wofsy, 2011). Because we found in our prior work that the surface dataset provides the strongest constraint on the spatial distribution of N_2O emissions (Wells et al., 2015), we employ these in the inversion and reserve the airborne data for a posteriori evaluation.

Fig. 1 shows a map of the surface measurement sites used in this study. The surface measurements consist primarily of discrete air-filled flasks from NOAA's Cooperative Global Air Sampling Network (CCGG) program (Dlugokencky et al., 1994); we also include flask-based air samples from the Commonwealth Scientific and Industrial Research Organisation (CSIRO) network, the Environment Canada (EC) network, and a National Institute of Water and Atmospheric research (NIWA) site. We assume a measurement uncertainty of 0.4 ppb at all flask sampling sites based on recommendations from the data providers. In addition to the flask-based air samples, we use high-frequency N_2O measurements (discrete hourly or hourly averaged) from the NOAA Chromatograph for Atmospheric Trace Species (CATS) network (Hall et al., 2007), the Advanced Global Atmospheric Gases Experiment (AGAGE) network (Prinn et al., 2000), and the University of Minnesota tall tower ~~Trace Gas Observatory~~ (~~TGO~~KCMP tall tower; Griffis et al., 2013; Chen et al., 2016). The hourly measurement uncertainty at these sites is approximately 0.3 ppb, 0.6 ppb, and 1 ppb, respectively.

Small calibration offsets between measurement networks can significantly impact N_2O inversions due to its low ambient variability relative to background mixing ratios. To address this, we adjust here the AGAGE and EC data to the same NOAA 2006A scale used by the NOAA CCGG, CATS, CSIRO, NIWA, and ~~TGO~~ KCMP measurements. For AGAGE, we calculate

an adjustment factor based on co-located CCGG flask-based air samples taken within 15 minutes of an in situ measurement at five sites: CGO (Cape Grim, Australia), MHD (Mace Head, Ireland), RPB (Ragged Point, Barbados), SMO (Tutuila, American Samoa), and THD (Trinidad Head, California). The mean CCGG:AGAGE ratio at these sites from 2010 to 2012 is 1.00037, and we apply this adjustment to all AGAGE data. For EC, we calculate an adjustment factor based on co-located NOAA flask-based air measurements at ALT (Alert, Nunavut). The mean NOAA:EC ratio during our analysis period is 1.00017, and we use this adjustment factor across the EC network. While calibration scale offsets can be concentration- and time-dependent, our relatively short (2-year) analysis window avoids the need for any temporally resolved measurement adjustments. Prior to our analysis we also screen for outliers by omitting any measurements more than two standard deviations (calculated on a running basis with a 30-day time window for flask-based air measurements and a 24-hour time window for in situ observations) away from its nearest neighbor.

For a posteriori evaluation of the inverse modeling results we employ airborne measurements from the HIPPO campaigns (Wofsy, 2011), which featured pole-to-pole sampling and regular vertical profiling from approximately 300 to 8500 m altitude, with some profiles extending to 14000 m. Figure 1 shows flight tracks for the two deployments occurring during our simulation period and used here: HIPPO IV (June-July 2011) and HIPPO V (August-September 2011). The aircraft payload included high-frequency N_2O measurements by quantum cascade laser spectroscopy (QCLS; Kort et al., 2011). To ensure calibration consistency we apply an offset adjustment to these data for each deployment based on concurrent flask-based air samples~~, taken using an onboard Whole Air Sampler (WAS)~~which are anchored to the NOAA 2006A scale.

3 Inversion sensitivity to initial conditions for N_2O

Because of the ~127 year atmospheric lifetime for N_2O, any bias in the model initial conditions can persist throughout the analysis period and lead to substantial errors in top-down emission estimates (Thompson et al., 2014c). In this section, we evaluate six alternate approaches to generating initial N_2O mass fields for the start date of our inversions (1 April 2010), their impact on the derived fluxes, and their overall suitability for inverse modeling.

The six treatments are summarized in Table 1. Three involve interpolation of surface observations from the NOAA, AGAGE, CSIRO, EC, and NIWA networks for alternate time windows (MarZonal, AprZonal, AprKriging), ~~and t~~wo~~hree~~ involve 4D-Var adjoint optimization of the initial mass field based on those same observations plus those from ~~TGO~~KCMP tall tower~~-~~ (AprOpt, FebOpt), and one involves optimization of the initial mass field based on observations from remote sites (RemoteOpt). Interpolation of observations offers the advantage of avoiding any model information that may bias the initial state, whereas a 4D-Var optimization of the initial conditions allows us to exploit subsequent atmospheric transport to inform the initial state in locations without N_2O observations. The first three approaches employ either linear interpolation of zonally-averaged surface measurements or Kriging, and use observations from March 2010 (with subsequent one month model spin-up) or from 25 March to 7 April 2010 (with no subsequent spin-up). In each case, the resulting surface mixing ratios of N_2O (mapped in Fig. S4) are assigned to all vertical levels in the troposphere; initial N_2O mixing ratios above 100

hPa are based on interpolated mean profiles from the EOS Aura Microwave Limb Sounder (MLS; Lambert et al., 2007). Where necessary, N_2O mixing ratios above the tropopause but below 100 hPa are linearly interpolated between the tropospheric and MLS values.

The three tests in which the initial conditions are optimized by 4D-Var use a time window of February-March 2010, April-May 2010, or January-June 2010 to solve for the initial N_2O mass field on 1 April 2010. Two of these assimilate all surface observations while one employs only data from remote sites. Below, we evaluate each of the six initial condition treatments against observations at the beginning of the simulation period (1-7 April 2010) and perform a standard 4D-Var optimization of N_2O emissions to quantify the sensitivity of the inferred fluxes to the selected initial conditions.

Table 2 shows ~~the~~ initial bias statistics with respect to ~~the~~ all surface observations and by hemisphere for each initial condition treatment. Of the interpolation approaches, the MarZonal setup has the poorest performance, with an overly strong interhemispheric gradient (the model is biased high in the Northern Hemisphere and low in the Southern Hemisphere) and the largest initial model:measurement bias at all sites. In this case, the 1-month model spinup, meant to smooth out any artificial N_2O gradients from the interpolation, is counterproductive as it allows model emission biases to accumulate prior to the inversion. The interpolation methods without subsequent spinup (AprZonal, AprKriging) perform better in terms of initial model:measurement bias – in the global mean and in each individual hemisphere ~~and the interhemispheric N_2O gradient.~~ We see the same general behavior when using 4D-Var to optimize the initial conditions, with the no-spinup AprOpt approach providing the lowest initial model:measurement bias (and least spread in bias) across all of the six methods tested. Using only data from remote sites (RemoteOpt) in the initial field optimization leads to a negative model bias, on average, in both hemispheres.

The bias statistics above can only test the realism of the initial N_2O fields in those locations where there are observations, and say nothing about any potential bias in the large majority of model grid squares that lack observations. On the other hand, by carrying out a full forward model run based on each of those initial conditions, we can exploit atmospheric transport to more fully assess the fidelity of the initial N_2O mass field based on the evolution of model:measurement biases at the various observation sites.

Fig. 2 shows monthly-mean model-measurement residuals (averaged for Northern and Southern Hemisphere sites) for a full two-year forward simulation using the a priori emissions for each of the above initial mass fields. While most of the initial conditions exhibit minimal bias at the start of the simulation, some develop large biases over time. As a result, the corresponding a posteriori global flux obtained in a 4D-Var source inversion (values shown inset in Fig. 2) varies considerably depending on the initial N_2O field, with the flux adjustment even changing sign: a posteriori values range from 16.1 to 21.4 Tg N yr^{-1}, i.e. from a ~7% reduction to a 23% increase in the prior flux. We see in Fig. 2 that the direction of the global flux adjustment corresponds to the trend in the model-measurement residuals. For example, with the MarZonal initial conditions, a significant negative trend in the residuals drives a global flux increase relative to the a priori, despite the fact that this case exhibits a positive mean bias with respect to the observations at the outset (Table 2). Such a trend in the model:measurement residuals could theoretically arise from ~~incorrect initial conditions or from~~ the accumulation of model

source/sink errors over the course of the simulation. However, ~~because~~ our a priori flux and lifetime are broadly consistent with independent observational constraints (Prather et al., 2012), whereas an annual N_2O source of 20+ Tg N would yield a higher-than-observed atmospheric growth rate~~.~~ ~~A~~a biased initial mass field is thus the more tenable explanation for the negative model:measurement residual trend.

Overall, the three simulations using initial conditions optimized by 4D-Var yield a relatively small trend in the model-measurement N_2O residuals, as does the AprZonal simulation, arguing for a more realistic initial N_2O distribution in these cases. While the a posteriori flux between them varies, differences are less than 10% of the a priori flux. Because the AprOpt initial conditions exhibit the lowest initial bias, along with the lack of a trend in the residual timeline, we choose this method to construct the initial conditions for the N_2O inversions presented here. Likewise, for future work on N_2O and other long-lived species, we recommend constructing the initial conditions by 4D-Var assimilation of observations at the outset of the inversion period. Because they are used for initial condition optimization, the April-May 2010 surface observations are excluded from the subsequent source inversions.

4 Inversion evaluation and results

Figure 3 shows maps of our derived annual a posteriori N_2O emissions from the standard, continental-scale, and SVD-based inversion for 2011, along with bar charts of the 2011 annual flux for the nine regions considered in the continental-scale inversion (numerical values listed in Table 3). A priori emissions, along with a posteriori emission increments (a posteriori-a priori difference) are also included for comparison. We focus on 2011 results to minimize any residual bias from the initial conditions. Focusing on 2011 also excludes the last three months of the inversion window~~, as~~ when the adjoint forcing weakens ~~towards the end of the simulation~~ due to the long lifetime of N_2O (Wells et al., 2015).

The optimized global fluxes, listed inset in each map in Fig. 3, range from 15.9 Tg N yr^{-1} for the SVD-based inversion to 17.5 – 17.7 Tg N yr^{-1} for the standard and continental-scale inversions, with some similar spatial patterns and some discrepancies that we explore further in Section 4.3. The SVD-based global flux agrees well with that implied by ~~its atmospheric~~ the N_2O lifetime and global burden for 2010 (15.7 ± 1.1 Tg N yr^{-1}; Prather et al., 2012). It also gives a better comparison to HIPPO IV and V measurements in the southern extratropics and to HIPPO V in the northern extratropics (see below~~, and thus appears to provide the best estimate of the true global flux~~. However, all three a posteriori global annual fluxes are close to or within the range of recent inverse studies (16.1-18.7 Tg N yr^{-1}). Below we evaluate our inversion results using aircraft and surface observations before interpreting them in terms of the information they provide on N_2O emission processes.

Formatted: Subscript

4.1 A posteriori evaluation of N_2O emissions

We apply the HIPPO IV and V airborne measurements described in Section 2.4 (and mapped in Fig. 1) to evaluate the a posteriori fluxes from our different inversion methods, and assess which method yields the most realistic depiction of true

N_2O fluxes. Figure 4 shows average vertical profiles of the model-measurement N_2O difference for these deployments in the a priori and the three inverse estimates ~~(standard 4D-Var, continental-scale, and SVD-based inversions)~~ as a function of latitude. Initially, the model vertical profile is biased high throughout the troposphere in the northern mid-to-high latitudes; this bias is larger during HIPPO V than HIPPO IV due to a seasonal bias in model emissions that is further discussed in Section 4.4. In the southern mid-to-high latitudes the model is also biased high through most of the troposphere. In most cases in Fig. 4 we see that the model-measurement difference trends negative with height in the troposphere, which may reflect a model underestimate of the convective transport of N_2O emissions (Kort et al., 2011). Large biases above 400 hPa in HIPPO IV (30° to 90° N) and HIPPO V (30° to 90° S) are driven by high latitude observations in which the aircraft is sampling below the model tropopause but above the actual tropopause, and highlight the difficulty in modeling the N_2O vertical profile at these altitudes.

All three inversions significantly reduce the 30° to 90° N bias seen for both HIPPO campaigns; the SVD-based approach provides the fullest correction during HIPPO V, while slightly overcorrecting the HIPPO IV bias. However, the high bias from 30° to 90° S is only reduced in the SVD-based inversion, despite the fact that the continental-scale inversion has the lowest a posteriori emissions in this latitude range (Table 3). The lower global flux obtained with the SVD-based approach (Fig. 3 and Table 3) is thus the reason for this correction, implying that the global annual a priori flux (from all sources combined) ~~is~~ may be too high. We note that a slight low bias does emerge in the tropics in the SVD-based approach, where ~~the spatial distribution of emissions is particularly difficult to resolve~~observational constraints are low.

4.2 Averaging kernel

The information from the randomized-SVD algorithm can be used to directly calculate the inversion averaging kernel (AK) and posterior error via Eqs. (3) and (4), giving valuable information on the spatial distribution of emission constraints provided by the N_2O observing network. Figure 5 shows the diagonal of the AK for N_2O emissions in April 2011 (results for other months are very similar). AK diagonal values near 1.0 indicate emission locations that are well-constrained by observations, while AK diagonal values close to 0 indicate emission locations that lack a direct constraint.

AK diagonal values for monthly N_2O emissions are highest in the US and Europe where the observational coverage is most extensive, with values up to 0.7 in locations where hourly observations are available. Weaker constraints are achieved in East Asia and some tropical and Australian grid boxes, with AK values ranging from 0.01-0.4. AK values throughout most of the Tropics, Southern Hemisphere, Canada, and northern Asia reveal almost no direct observational constraints on monthly emissions in these regions.

The number of pieces of information that can be independently resolved (DOFs) in any inversion can be determined from the trace of the AK. Here, the DOFs are ~315 for the full two-year inversion. A key advantage of the SVD-based approach is that it solves for only those spatiotemporal flux patterns that can be constrained by the observations: i.e., the dimension of the solution is consistent with the DOFs of the inversion. On the other hand, the standard inversion attempts to resolve 79,466 free variables, ~250× more than can legitimately be constrained, while the continental-scale inversion yields fewer

pieces of information (216) than are obtainable. The latter point confirms that the observations can in fact resolve some finer-scale spatial and temporal information on N_2O emissions in the regions where AK values are highest.

4.3 Regional annual N_2O emissions

In this section we interpret the inversion results by region in terms of their implications for present understanding of N_2O emission processes. We focus on the spatial information obtained from the standard and SVD-based inversions and on those features that are most robust across these inversion frameworks.

4.3.1 North America

A posteriori emissions from North America range from 1.24-1.78 Tg N yr^{-1}, with a slight increase (11%) inferred relative to the a priori inventory for the continental-scale inversion versus a 20-23% decrease for the standard and SVD-based inversion. The latter values are quite close to a recent estimate from Saikawa et al. (2014) for 2008 (1.2 ± 0.2 Tg N yr^{-1}). Both the standard and SVD-based inversions call for a large increase (2-3×) in emissions from the US corn belt (Fig. 3), one of the most intensively managed agricultural regions of the world. The magnitude of this upward adjustment supports emission underestimates previously found for this region (Kort et al., 2008; Miller et al., 2012; Griffis et al., 2013), and ~~is likely due~~ which has been attributed to underrepresentation of ~~the~~ indirect N_2O ~~source~~ emissions following ~~associated with~~ leaching and runoff from agricultural soils (Turner et al., 2015; Chen et al., 2016). However, other processes could also contribute, such as freeze-thaw emissions or direct emissions after spring fertilizer application. The timing of these processes, and that of peak stream flow, correspond to the dominant modes of ambient N_2O variability observed in this region (Griffis et al., 2017). Finally, we find that e~~E~~missions decrease relative to the a priori estimate in the western US and Canada (in both the standard and SVD inversions), where natural soil emissions may be too high in the CLMCN-N_2O inventory (Saikawa et al., 2014) used here, and where recent work argues that direct agricultural emissions are overestimated using a standard linear emission model (Gerber et al., 2016) ~~as a priori.~~

Formatted: Subscript

4.3.2 South America

A posteriori emissions from South America range from 3.28-3.68 Tg N yr^{-1}, increasing 6-19% over the a priori. These values are 40-60% larger than the median inferred by Thompson et al. (2014c) for 2006-2008 (2.33 Tg N yr^{-1}); however, due to weak observational constraints (Fig. 5) we find that the results here are quite sensitive to the inversion framework used. For example, including fewer modes in the SVD-based solution yields an even higher a posteriori flux in this region, and the spatial distribution of emissions differs substantially between the standard and SVD-based solutions. Saikawa et al. (2014) do note a large recent increase in nitrogen fertilizer consumption over this region (49% from 1995-2008), which may help explain the larger a posteriori flux seen here, although N fertilizer use in this region was only 7% of the global total in 2011 (International Fertilizer Association, 2016).

4.3.3 Europe

All three inversions point to a significant model overestimate of European N_2O emissions, with a posteriori fluxes that are 38% (standard inversion; optimized flux 1.05 Tg N yr^{-1}) to 75% (SVD-based inversion; optimized flux 0.43 Tg N yr^{-1}) lower than the a priori. These optimized fluxes are in better agreement with the other top-down flux estimates for Europe (both for 2006) of 1.19 Tg N yr^{-1} (Corazza et al., 2011) and 0.93 ±0.12 Tg N yr^{-1} (Saikawa et al., 2014). The European source derived in the SVD-based and continental-scale inversions (0.43-0.57 Tg N yr^{-1}) represents ~3% of the global flux found in each case, which agrees with the result from Huang et al. (2008). We find the largest emission reductions over western and central Europe, suggesting an overestimate of soil and non-agricultural anthropogenic sources in the EDGARv4.2 inventory used here. While non-agricultural anthropogenic sources ~~provide a small contribution to the~~make up only ~10% of the global a priori N_2O flux ~~(~13%)~~, they comprise ~340% of the European a priori model emissions. ~~European emissions in the model~~. ~~Furthermore, b~~Based on the spatial distribution of the adjustments derived in the ~~standard and SVD-based adjustments~~inversions, ~~this~~ we find that both of these sources (soils, non-agricultural anthropogenic) have a comparable high bias (from 40-70% as indicated by the standard and SVD-based inversions, respectively) in the a priori inventories over Europe.~~undergoes a larger relative reduction than the soil source when integrated over Europe as a whole.~~

4.3.4 Africa

Annual emissions from Africa range from 2.85-2.97 Tg N yr^{-1} in all three inversions, an 8-12% increase from the prior flux. Our a posteriori values are closer to the median optimized African flux found by Thompson et al. (2014c) for 2006-2008 (3.36 Tg N yr^{-1}) than is the a priori; however, the lack of direct observational constraints for this region (Fig. 5) prevent any definitive conclusion. As in South America, the SVD-based result here is quite sensitive to the number of modes used, with emission increments differing in sign for some months. The spatial distribution between the standard and SVD-based solutions also differs, with the former preserving the a priori distribution and the latter placing more of the flux in equatorial Africa.

4.3.5 Asia

Over Asia the a posteriori flux ranges from 3.82 Tg N yr^{-1} (9% decrease from the a priori) to 4.59 Tg N yr^{-1} (10% increase). The full-dimensional and SVD-based inversions both call for a reduction in model emissions for northern China and Russia and an increase to the south. Consistent a posteriori spatial patterns emerge in the latter region, with large emission increases over the prior for the Indo-Gangetic Plain (IGP) of India, Southeast Asia, and Eastern China. Our flux estimates are towards the higher end of the wide range of estimates for North + South Asia (2.87-4.48 Tg N yr^{-1}) reported by Thompson et al. (2014c) for 2006-2008; that study concludes that observational constraints are low in this region, which is generally consistent with our findings (Fig. 5). Saikawa et al. (2014) find that agricultural N_2O emissions are increasing in South Asia, and that is consistent with our higher flux for 2011 compared to the Thompson et al. (2014c) median value for 2006-2008.

58% of global N fertilizer consumption occurred in South and East Asia in 2011 (International Fertilizer Association, 2016); it is possible that direct, on-field N_2O emissions here are underestimated ~~due to the nonlinear increase in emissions as~~with N inputs exceeding crop demands (Shcherbak et al, 2014). Indeed, a recent bottom-up estimate derives a direct emission response for China that is 42% larger than the global average (Gerber et al., 2016). Over northern Asia our results point to an overestimate of natural soil emissions (as this is the dominant regional source in the model); a similar overestimate was inferred by Saikawa et al. (2014) ~~using the same a priori inventory~~.

4.3.6 Oceania

The emission estimates for Oceania range from 0.64 Tg N yr^{-1} (16% decrease from the prior) to 0.84 Tg N yr^{-1} (10% increase). Observational constraints are low in this region (outside of Cape Grim, where a measurement site exists, Fig. 5) and results depend strongly on the a priori. The weak emission reduction ~~seen~~ in the continental-scale inversion (~~Fig.~~Table 3) could also reflect a model overestimate of the southern ocean source, as the sparse observations make it difficult to separate land versus ocean emissions here.

4.3.7 Ocean emissions

We obtain an annual flux ranging from 0.07-0.52 Tg N yr^{-1} for northern oceans (30° – 90° N), 2.19-2.99 Tg N yr^{-1} for tropical oceans (30° S – 30° N), and 0.39-0.70 Tg N yr^{-1} for southern oceans (30° – 90° S). In all cases, our results indicate an emission increase for tropical oceans emissions (of 9-47%) and a decrease for northern (20-90%) and southern (11-51%) oceans relative to the a priori Jin and Gruber (2003) inventory. The wide range of values reflects the limited degree to which the surface observing network can constrain ocean emissions. However, the standard and SVD-based inversions both point to a model overestimate in the North Atlantic where downwind observations in Europe have some power to resolve monthly emissions.

The direction of the oceanic emission changes is consistent with the findings of Thompson et al. (2014c); however, our oceanic fluxes are lower than obtained in that study (1.08, 3.66, and 1.20 Tg N yr^{-1} for northern, tropical, and southern oceans, respectively). Compared to Thompson et al. (2014c), ~~R~~results obtained here (3.38-3.45 Tg N yr^{-1}) are ~~more consistent with~~closer to the most recent best estimate of the oceanic source derived from ~~global~~ observations of the air-sea N_2O gradient (2.4 ± 0.8 Tg N yr^{-1}; Buitenhuis et al., 2017), albeit still higher. We find that ocean emissions make up ~20% of the global N_2O flux (in both the a priori and a posteriori estimates), lower than found in some inverse studies (31-38%; Saikawa et al., 2014; Thompson et al., 2014c) but consistent with Huang et al. (2008) (~23%).

4.3.7 Summary of regional scale results

Among the most robust spatial features of our results across all the inversion frameworks employed is an increase in annual N_2O emissions over the a priori in the tropics (particularly 0°-30° N), and a decrease at higher latitudes for both ocean and terrestrial sources. While the total Asian flux differs between the full-dimensional and SVD-based inversion, both solutions

indicate a model overestimate in northern Asia and an underestimate in Southeast Asia. Furthermore, while the inversions disagree on whether the a priori emissions are too high or too low over North America as a whole, both the full-dimensional and SVD-based inversions increase the prior N_2O emissions over the US corn belt and reduce them over the western US and Canada. This suggests that while the a priori emissions may be too high in northern mid-to-high latitudes overall (which we attribute to overly-high natural soil emissions in the model, as well as non-agricultural anthropogenic emissions in regions such as Europe, and a possible overestimate of direct emissions in drier regions) they are underestimated for fertilized agricultural soils in the US Corn Belt and likely also in Asia.

4.4 Seasonality of N_2O emissions

4.4.1 A priori seasonality

Figure 2 shows that the a priori model bias in atmospheric N_2O varies strongly as a function of season in the Northern Hemisphere, implying a corresponding seasonal bias in the bottom-up emissions driving the model. Because the EDGARv4.2 emissions used here are annual, the ~~S~~seasonality in our prior emissions over land is dominated by the natural soil source. Here, we compare the temporal constraints afforded by the different inversions, focusing again on the most robust features across the inversions, after first examining the seasonality differences between modeled and measured N_2O mixing ratios.

Figure 6 shows two-year timelines of monthly-averaged a priori modeled and measured N_2O mixing ratios along with the corresponding model-measurement residual for all surface measurement sites. The modeled N_2O from 30° – 90° N is characterized by a November – December peak, and a May – June minimum. This is out of phase with the measurements, which have a minimum around August – September and a peak in February – March. Several other CTMs in ~~an~~ a recent intercomparison (Thompson et al., 2014b; 2014c) likewise produce a seasonal minimum that is too early compared to observations, which that study suggests may reflect an overestimate of the impact of N_2O-depleted stratospheric air on surface mixing ratios. Our previous work indicates that surface N_2O mixing ratios are not sensitive to biases in the magnitude of the stratospheric sink on the timescale of our inversion (Wells et al., 2015), while Thompson et al. (2011) find that errors in modeled stratosphere-troposphere exchange ~~(STE)~~ can bias inferred regional emissions by up to 25%, particularly over the North Atlantic and Europe. We thus focus here on inferred seasonal changes that are significantly larger than 25% and most robust to any potential errors in modeled ~~STE~~stratosphere-troposphere exchange.

Measured mixing ratios at the KCMP tall tower site in Minnesota are significantly higher than other Northern Hemisphere sites. As a result, it is one of the few sites where negative model-measurement residuals persist through most of the two-year inversion period. ~~The fact that it is also one of the only sites located in an agricultural source~~Located in an agricultural region composed mainly of drained lands, the low model bias is consistent with ~~region provides support for~~ previous findings of a missing or strongly underestimated agricultural N_2O source tied to indirect emissions (Griffis et al., 2013; Chen et al., 2016).

4.4.2~~1~~ Seasonality of N_2O inversion results

Figure 7 contains 2011 timelines of the monthly a priori and a posteriori emissions for the three inversion methods over the same continental and ocean regions considered above. Both North American and European a posteriori emissions are characterized by a shift from a summertime (June-July) to springtime peak in emissions (March-April), with the North American results exhibiting separate spring and summer peaks (plus a ~~fall winter~~ n October enhancement in the SVD-based inversion). The a posteriori seasonality over Asia is nearly reversed from the a priori, with dual emission peaks in spring (March-May~~April~~) and fall (September-October). This double maximum is consistent with past work and coincides with the approximate start and end times of the Asian monsoon (Thompson et al., 2014c). Over South America and Africa we find that the a posteriori seasonality depends more strongly on the inversion method used, reflecting the low observational constraints in these regions (Fig. 5). Tropical ocean emissions increase primarily during summer and fall when emissions are at their peak, though the magnitude ~~depends on the inversion method used~~varies across inversion frameworks. Emissions decrease strongly for the northern oceans (though they were not large to begin with) for the continental and SVD-based inversions, but with no shift in seasonality. Seasonal emission adjustments are small over the southern oceans and Oceania, where constraints are weak.

The shift toward earlier springtime emissions in the Northern Hemisphere is one robust feature across our inversions. Thompson et al. (2014c) arrived at the same finding, and argued that it reflects the dependence of N_2O emissions on soil moisture and temperature, as drier soils later in summer may limit N_2O fluxes. However, other factors are also likely to contribute. Emissions associated with freeze-thaw cycles can lead to elevated springtime N_2O fluxes at these mid- to high-latitudes (e.g., Wagner-Riddle et al., 2017), while higher springtime emissions are also consistent with the timing of fertilizer application and indirect N_2O emissions due to leaching and runoff ~~from agricultural soils~~when streamflow is at its peak (Chen et al., 2016; Griffis et al., 2017). The separate spring and summer emission peaks seen over North America in 2011 may reflect the respective influences of indirect and direct emissions, which have been shown (Chen et al., 2016) to peak earlier (indirect emissions) and later (direct emissions) in the growing season. Fall fertilizer application is also common in the US Corn Belt—more than one third of corn farmers in Minnesota do their main N application during this time (Beirman et al., 2012)—which could explain the October peak in the SVD-based results, and provide a source of nitrogen that would be released in the early spring thaw and subsequent runoff period.

We see in Fig. 7 that the seasonal adjustments are larger in the continental and SVD-based inversion than the standard 4D-Var, particularly in regions where direct observational constraints are low. In our previous work (Wells et al., 2015) we highlighted the difficulty in correcting seasonal biases when solving for monthly N_2O emissions on a grid box scale. The SVD-based approach thus provides a major advantage in this context, by reducing the dimensions of the inverse problem and allowing us to better resolve temporal features that inform our understanding of N_2O emission processes.

5 Conclusions and implications for the N_2O budget

In this paper we employed three inversion frameworks to derive top-down constraints on global~~,~~ monthly N_2O emissions for 2011. The inverse frameworks included: (1) a standard 4D-Var inversion at 4° × 5°, (2) a 4D-Var inversion solving for fluxes on six continental and three ocean regions, and (3) a fast 4D-Var inversion based on a new dimension reduction technique using efficient randomized SVD algorithms. The latter technique is an advance over ~~arbitrary~~ typical aggregation schemes: ~~the~~ it defines the optimal resolution of the solution ~~is defined quantitatively~~ according to the information afforded by the observations; ~~the~~ is maximizes the DOFs of the inverse system ~~are maximized~~; and offers major time savings ~~are achieved~~ compared to other iterative inversion methods.

Over many regions, our inversion results are broadly consistent with other recent inversion studies, though the range of derived flux values and seasonalities from poorly-observed regions highlights the ill-posed nature of the inverse problem for N_2O. Based on the most robust features across our three different inversion frameworks, we can draw the following conclusions about the global N_2O budget and underlying emission processes:

- The global annual N_2O flux is likely somewhat high in the bottom-up inventory used here, as the lower value (15.9 Tg N yr^{-1}) derived in the SVD-based inversion gives a better representation of the N_2O background in the extratropics while also being more consistent with the current best estimate from a 0-D consideration of the global burden and lifetime of N_2O (Prather et al., 2012).
- Our inversion results indicate that a greater fraction of the global N_2O flux is emitted from the tropics than the a priori inventories would suggest. This points to an overestimate of natural soil (and perhaps industrial/residential) emissions in the Northern Hemisphere, and to an underestimate of agricultural (and likely oceanic) emissions in the tropics. The former hypothesis would be consistent with the 2-fold reduction in the industrial N_2O source for EDGAR versions subsequent to that used here.
- In the Northern Hemisphere midlatitudes, N_2O emissions peak ~~earlier in the year~~in the springtime (March-April) ~~than our current inventories suggest (June-July).~~ This seasonality is ~~consistent with~~supported by other recent studies and corresponds to the period of higher soil moisture, peak streamflow, ~~and~~ thawing of frozen soils ~~in the springtime~~, and with the timing of fertilizer application.
- We find that N_2O emissions from agricultural soils are underestimated in the US Corn belt and likely also in Asia.~~,~~ ~~and that this~~We attribute this ~~is likely due~~ to an underestimate of indirect agricultural emissions ~~during early spring and summer~~due to leaching and runoff, ~~in the Northern Hemisphere.~~ freeze-thaw emissions in early spring, and the direct on-field source when N inputs exceed crop demands. ~~For example, a~~Annual emissions over the US Corn Belt are underestimated by 2-3× in the a priori inventories; the standard and SVD-based inversions used here both increase emissions from this region throughout the growing period (March – September).

Based on our analysis of alternate initial conditions for atmospheric N_2O, and their corresponding effects on derived fluxes, we recommend formally optimizing the initial mass field (either alone or in tandem with the emissions optimization) rather

Formatted: Normal, No bullets or numbering

Formatted: Subscript

than interpolating N_2O observations or using an unconstrained model spinup. The impacts can be substantial: for the sensitivity tests used here, a posteriori global fluxes ranged by ~25% (16.1 – 21.4 Tg N yr^{-1}) across different treatments of the initial N_2O mass.

Finally, the SVD-based inverse approach used here offers a powerful framework for maximizing the emission information derived from atmospheric observations of N_2O in an efficient, timely manner, particularly for models with a low level of parallelization. The approach provides valuable spatially-resolved information that is lost when solving for fluxes over ad-hoc continental-scale regions, while also providing a much stronger ability to resolve broad temporal features than is possible with a standard 4D-Var inversion at the model grid resolution. Such information is key to furthering our understanding of N_2O emission processes based on top-down analyses.

Code availability

The N_2O version of the GEOS-Chem adjoint code is available via the GEOS-Chem adjoint repository. Instructions for obtaining access to the code can be found at http://wiki.seas.harvard.edu/geos-chem/index.php/GEOS-Chem_Adjoint.

Appendix A: Proof for cost function projection formula

$$J(\boldsymbol{x}) = \frac{1}{2}(\boldsymbol{h}(\boldsymbol{x}) - \boldsymbol{y})^T \mathbf{S}_y^{-1}(\boldsymbol{h}(\boldsymbol{x}) - \boldsymbol{y}) + \frac{1}{2}(\boldsymbol{x} - \boldsymbol{x}_a)^T \mathbf{S}_a^{-1}(\boldsymbol{x} - \boldsymbol{x}_a), \quad \text{(A1)}$$

and

$$\boldsymbol{h}(\boldsymbol{x}) = \boldsymbol{h}(\boldsymbol{x}_a) + \mathbf{H}(\boldsymbol{x} - \boldsymbol{x}_a), \quad \text{(A2)}$$

Therefore,

$$(\boldsymbol{h}(\boldsymbol{x}) - \boldsymbol{y})^T \mathbf{S}_y^{-1}(\boldsymbol{h}(\boldsymbol{x}) - \boldsymbol{y}) = (\boldsymbol{h}(\boldsymbol{x}_a) + \mathbf{H}(\boldsymbol{x} - \boldsymbol{x}_a) - \boldsymbol{y})^T \mathbf{S}_y^{-1}(\boldsymbol{h}(\boldsymbol{x}_a) + \mathbf{H}(\boldsymbol{x} - \boldsymbol{x}_a) - \boldsymbol{y}) = \left(\boldsymbol{h}(\boldsymbol{x}_a) + \mathbf{S}_y^{\frac{1}{2}} \mathbf{S}_y^{-\frac{1}{2}} \mathbf{H} \mathbf{S}_a^{\frac{1}{2}} \mathbf{S}_a^{-\frac{1}{2}} (\boldsymbol{x} - \boldsymbol{x}_a) - \boldsymbol{y}\right)^T \mathbf{S}_y^{-1} \left(\boldsymbol{h}(\boldsymbol{x}_a) + \mathbf{S}_y^{\frac{1}{2}} \mathbf{S}_y^{-\frac{1}{2}} \mathbf{H} \mathbf{S}_a^{\frac{1}{2}} \mathbf{S}_a^{-\frac{1}{2}} (\boldsymbol{x} - \boldsymbol{x}_a) - \boldsymbol{y}\right), \quad \text{(A3)}$$

Then we develop $\mathbf{S}_y^{-\frac{1}{2}} \mathbf{H} \mathbf{S}_a^{\frac{1}{2}} = \sum_{i=1}^{n} \lambda_i^{\frac{1}{2}} \boldsymbol{w}_i \boldsymbol{v}_i^T$, where n is the dimension of the state vector, and project the control variable onto the optimal basis $\{\mathbf{S}_a^{\frac{1}{2}} \boldsymbol{v}_i, i = 1, \ldots, k\}$ using the projector $\pi = \mathbf{S}_a^{\frac{1}{2}} \sum_{i=1}^{k} \boldsymbol{v}_i \boldsymbol{v}_i^T \mathbf{S}_a^{-\frac{1}{2}}$, which yields:

$$(\boldsymbol{h}(\boldsymbol{x}) - \boldsymbol{y})^T \mathbf{S}_y^{-1}(\boldsymbol{h}(\boldsymbol{x}) - \boldsymbol{y}) \approx (\boldsymbol{h}(\boldsymbol{x}_a) - \boldsymbol{y})^T \mathbf{S}_y^{-1}(\boldsymbol{h}(\boldsymbol{x}_a) - \boldsymbol{y}) + (\boldsymbol{x} - \boldsymbol{x}_a)^T \mathbf{S}_a^{-\frac{1}{2}} \sum_{i=1}^{k} \lambda_i \boldsymbol{v}_i \boldsymbol{v}_i^T \mathbf{S}_a^{-\frac{1}{2}} (\boldsymbol{x} - \boldsymbol{x}_a) + (\boldsymbol{h}(\boldsymbol{x}_a) - \boldsymbol{y})^T \mathbf{S}_y^{-\frac{1}{2}} \sum_{i=1}^{k} \lambda_i^{\frac{1}{2}} \boldsymbol{w}_i \boldsymbol{v}_i^T \mathbf{S}_a^{-\frac{1}{2}} (\boldsymbol{x} - \boldsymbol{x}_a) + (\boldsymbol{x} - \boldsymbol{x}_a)^T \mathbf{S}_a^{-\frac{1}{2}} \sum_{i=1}^{k} \lambda_i^{\frac{1}{2}} \boldsymbol{v}_i \boldsymbol{w}_i^T \mathbf{S}_y^{-\frac{1}{2}} (\boldsymbol{h}(\boldsymbol{x}_a) - \boldsymbol{y}), \quad \text{(A4)}$$

and

$$(\boldsymbol{x} - \boldsymbol{x}_a)^T \mathbf{S}_a^{-1}(\boldsymbol{x} - \boldsymbol{x}_a) \approx (\boldsymbol{x} - \boldsymbol{x}_a)^T \mathbf{S}_a^{-\frac{1}{2}} \sum_{i=1}^{k} \boldsymbol{v}_i \boldsymbol{v}_i^T \mathbf{S}_a^{-\frac{1}{2}} (\boldsymbol{x} - \boldsymbol{x}_a), \quad \text{(A5)}$$

Inserting Eqs. (A4) and (A5) in Eq. (A1), one obtains:

$$J(\boldsymbol{x}) \approx \frac{1}{2}(\boldsymbol{x}-\boldsymbol{x}_a)^T \mathbf{S}_a^{-\frac{1}{2}} \sum_{i=1}^{k} \boldsymbol{v}_i \boldsymbol{v}_i^T \mathbf{S}_a^{-\frac{1}{2}} (\boldsymbol{x}-\boldsymbol{x}_a) + \frac{1}{2}(\boldsymbol{h}(\boldsymbol{x}_a)-\boldsymbol{y})^T \mathbf{S}_y^{-1} (\boldsymbol{h}(\boldsymbol{x}_a)-\boldsymbol{y}) + \frac{1}{2}(\boldsymbol{x}-\boldsymbol{x}_a)^T \mathbf{S}_a^{-\frac{1}{2}} \sum_{i=1}^{k} \lambda_i \boldsymbol{v}_i \boldsymbol{v}_i^T \mathbf{S}_a^{-\frac{1}{2}} (\boldsymbol{x}-\boldsymbol{x}_a) + \frac{1}{2}(\boldsymbol{h}(\boldsymbol{x}_a)-\boldsymbol{y})^T \mathbf{S}_y^{-\frac{1}{2}} \sum_{i=1}^{k} \lambda_i^{\frac{1}{2}} \boldsymbol{w}_i \boldsymbol{v}_i^T \mathbf{S}_a^{-\frac{1}{2}} (\boldsymbol{x}-\boldsymbol{x}_a) + \frac{1}{2}(\boldsymbol{x}-\boldsymbol{x}_a)^T \mathbf{S}_a^{-\frac{1}{2}} \sum_{i=1}^{k} \lambda_i^{\frac{1}{2}} \boldsymbol{v}_i \boldsymbol{w}_i^T \mathbf{S}_y^{-\frac{1}{2}} (\boldsymbol{h}(\boldsymbol{x}_a)-\boldsymbol{y}), \quad \text{(A6)}$$

Differentiating Eq. (A6), one obtains:

$$\nabla J(\boldsymbol{x}) \approx \mathbf{S}_a^{-\frac{1}{2}} \sum_{i=1}^{k} \boldsymbol{v}_i \boldsymbol{v}_i^T \mathbf{S}_a^{-\frac{1}{2}} (\boldsymbol{x}-\boldsymbol{x}_a) + \mathbf{S}_a^{-\frac{1}{2}} \sum_{i=1}^{k} \lambda_i \boldsymbol{v}_i \boldsymbol{v}_i^T \mathbf{S}_a^{-\frac{1}{2}} (\boldsymbol{x}-\boldsymbol{x}_a) + \mathbf{S}_a^{-\frac{1}{2}} \sum_{i=1}^{k} \lambda_i^{\frac{1}{2}} \boldsymbol{v}_i \boldsymbol{w}_i^T \mathbf{S}_y^{-\frac{1}{2}} (\boldsymbol{h}(\boldsymbol{x}_a)-\boldsymbol{y}), \quad \text{(A7)}$$

Acknowledgements

This work was supported by NOAA (grant no. NA13OAR4310086 and NA13OAR4310081) and the Minnesota Supercomputing Institute. The KCMP measurements were made with support from the USDA (grant no. 2013-67019-21364). We thank E. Kort and S. Wofsy for providing the HIPPO N_2O measurements. We thank Environment Canada for providing data from the Alert, Churchill, Estevan Point, East Trout Lake, Fraserdale, and Sable Island Sites. We thank R. Martin and S. Nichol for providing data from the Arrival Heights NIWA station. We thank J. Muhle and C. Harth (UCSD-SIO), P. Fraser (CSIRO), R. Wang (GaTech), and other members of the AGAGE team for providing AGAGE data. The AGAGE Mace Head, Trinidad Head, Cape Matatula, Ragged Point, and Cape Grim stations are supported by NASA grants to the Massachusetts Institute of Technology and Scripps Institution of Oceanography; the Department of Energy and Climate Change (DECC, UK) contract to the University of Bristol; and by CSIRO and the Australian Bureau of Meteorology. We thank C. Adam Schlosser for work on the MIT IGSM.

References

Beaulieu, J. J., Tank, J. L., Hamilton, S. K., Wollheim, W. M., Hall, R. O., Mulholland, P. J., Peterson, B. J., Ashkenas, L. R., Cooper, L. W., Dahm, C. N., Dodds, W. K., Grimm, N. B., Johnson, S. L., McDowell, W. H., Poole, G. C., Valett, H. M., Arango, C. P., Bernot, M. J., Burgin, A. J., Crenshaw, C. L., Helton, A. M., Johnson, L. T., O'Brien, J. M., Potter, J. D., Sheibley, R. W., Sobota, D. J., and Thomas, S. M.: Nitrous oxide emission from denitrification in stream and river networks, P. Natl. Acad. Sci. USA, 108, 214-219, doi:10.1073/pnas.1011464108, 2011.

Beirman, P., Rosen, C., Venterea, R., and Lamb, J.: Survey of nitrogen fertilizer use on corn in Minnesota, Agr. Syst.,109, 43–52, 2012.

Bocquet, M., Wu, L., and Chevallier, F.: Bayesian design of control space for optimal assimilation of observations. Part I: Consistent multiscale formalism, Q. J. Roy. Meteor. Soc., 137, 1340-1356, doi:10.1002/qj.837, 2011.

Bousserez, N., and Henze, D. K.: Optimal and scalable methods to approximate the solutions of large-scale Bayesian problems: theory and application to atmospheric inversions and data assimilation, submitted, 2017.

Formatted: Font: (Default) +Body (Times New Roman), 1 pt
Formatted: Font: (Default) +Body (Times New Roman)
Formatted: Font: (Default) +Body (Times New Roman), 1 pt
Formatted: Font: 10 pt
Formatted: Font: 10 pt
Formatted: Font: 10 pt
Formatted: Font: 10 pt
Formatted: Font: 10 pt

Bouwman, A. F.: Environmental science - Nitrogen oxides and tropical agriculture, Nature, 392, 866-867, doi:10.1038/31809, 1998.

Bouwman, A. F., Beusen, A. H. W., Griffioen, J., Van Groenigen, J. W., Hefting, M. M., Oenema, O., Van Puijenbroek, P. J. T. M., Seitzinger, S., Slomp, C. P., and Stehfest, E.: Global trends and uncertainties in terrestrial denitrification and N_2O emissions, Philos. T. R. Soc. B, 368, 20130112, doi:10.1098/rstb.2013.0112, 2013.

Bui-Thanh, T., Burstedde, C., Ghattas, O., Martin, J., Stadler, G., Wilcox, L. C., and Ieee: Extreme-Scale UQ for Bayesian Inverse Problems Governed by PDEs, in: International Conference for High Performance Computing Networking Storage and Analysis, 25th ACM/IEEE International Conference for High Performance Computing, Networking, Storage and Analysis (SC), Salt Lake City, UT, 2012, WOS:000316911000003, 2012.

Buitenhuis, E. T., Suntharalingam, P., and Le Quéré, C.: Constraints on global oceanic emissions of N_2O from observations and models, Biogeosciences Discuss., in review, doi:10.5194/bg-2017-19, 2017.

Butterbach-Bahl, K., Baggs, E. M., Dannenmann, M., Kiese, R., and Zechmeister-Boltenstern, S.: Nitrous oxide emissions from soils: how well do we understand the processes and their controls?, Philos. T. R. Soc. B, 368, 20140122, doi:10.1098/rstb.2013.0122, 2013.

Byrd, R. H., Lu, P. H., Nocedal, J., and Zhu, C. Y.: A limited memory algorithm for bound constrained optimization, SIAM J. Sci. Comput., 16, 1190-1208, doi:10.1137/0916069, 1995.

Chen, Z. C., Griffis, T. J., Millet, D. B., Wood, J. D., Lee, X., Baker, J. M., Xiao, K., Turner, P. A., Chen, M., Zobitz, J., and Wells, K. C.: Partitioning N_2O emissions within the US Corn Belt using an inverse modeling approach, Global Biogeochem. Cy., 30, 1192-1205, doi:10.1002/2015gb005313, 2016.

Cohen, Y., and Gordon, L. I.: Nitrous oxide production in the ocean, J. Geophys. Res.-Oc. Atm., 84, 347-353, doi:10.1029/JC084iC01p00347, 1979.

Corazza, M., Bergamaschi, P., Vermeulen, A. T., Aalto, T., Haszpra, L., Meinhardt, F., O'Doherty, S., Thompson, R., Moncrieff, J., Popa, E., Steinbacher, M., Jordan, A., Dlugokencky, E., Bruehl, C., Krol, M., and Dentener, F.: Inverse modelling of European N_2O emissions: assimilating observations from different networks, Atmos. Chem. Phys., 11, 2381-2398, doi:10.5194/acp-11-2381-2011, 2011.

Crutzen, P. J., Mosier, A. R., Smith, K. A., and Winiwarter, W.: N_2O release from agro-biofuel production negates global warming reduction by replacing fossil fuels, Atmos. Chem. Phys., 8, 389-395, doi:10.5194/acp-8-389-2008, 2008.

Cui, T., Martin, J., Marzouk, Y. M., Solonen, A., and Spantini, A.: Likelihood-informed dimension reduction for nonlinear inverse problems, Inverse Probl., 30, doi:10.1088/0266-5611/30/11/114015, 2014.

Davidson, E. A.: The contribution of manure and fertilizer nitrogen to atmospheric nitrous oxide since 1860, Nature Geoscience, 2, 659-662, doi:10.1038/ngeo608, 2009.

Deng, F., Jones, D. B. A., Henze, D. K., Bousserez, N., Bowman, K. W., Fisher, J. B., Nassar, R., O'Dell, C., Wunch, D., Wennberg, P. O., Kort, E. A., Wofsy, S. C., Blumenstock, T., Deutscher, N. M., Griffith, D. W. T., Hase, F., Heikkinen, P.,

Sherlock, V., Strong, K., Sussmann, R., and Warneke, T.: Inferring regional sources and sinks of atmospheric CO_2 from GOSAT XCO_2 data, Atmos. Chem. Phys., 14, 3703-3727, doi:10.5194/acp-14-3703-2014, 2014.

Deng, F., Jones, D. B. A., Walker, T. W., Keller, M., Bowman, K. W., Henze, D. K., Nassar, R., Kort, E. A., Wofsy, S. C., Walker, K. A., Bourassa, A. E., and Degenstein, D. A.: Sensitivity analysis of the potential impact of discrepancies in stratosphere-troposphere exchange on inferred sources and sinks of CO_2, Atmos. Chem. Phys., 15, 11773-11788, doi:10.5194/acp-15-11773-2015, 2015.

Dlugokencky, E. J., Steele, L. P., Lang, P. M., and Masarie, K. A.: The growth rate and distribution of atmospheric methane, J. Geophys. Res.-Atmos., 99, 17021-17043, doi:10.1029/94jd01245, 1994.

Elkins, J. W., Wofsy, S. C., McElroy, M. B., Kolb, C. E., and Kaplan, W. A.: Aquatic sources and sinks for nitrous oxide, Nature, 275, 602 – 606, doi:10.1038/275602a0, 1978.

Firestone, M. K., and Davidson, E. A.: Microbiological basis of NO and N_2O production and consumption in the soil, in: Exchange of Trace Gases Between Terrestrial Ecosystems and the Atmosphere, edited by: Andreae, M. O., and Schimel, D. S., Wiley and Sons, Chichester, 7-21, 1989.

Flath, H. P., Wilcox, L. C., Akcelik, V., Hill, J., Waanders, B. V., and Ghattas, O.: Fast algorithms for Bayesian uncertainty quantification in large-scale linear inverse problems based on low-rank partial Hessian approximations, SIAM J. Sci. Comput., 33, 407-432, doi:10.1137/090780717, 2011.

Galloway, J. N., Townsend, A. R., Erisman, J. W., Bekunda, M., Cai, Z. C., Freney, J. R., Martinelli, L. A., Seitzinger, S. P., and Sutton, M. A.: Transformation of the nitrogen cycle: Recent trends, questions, and potential solutions, Science, 320, 889-892, doi:10.1126/science.1136674, 2008.

Gerber, J. S., Carlson, K. M., Makowski, D., Mueller, N. D., Garcia de Cortazar-Atauri, I., Havlík, P., Herrero, M., Launay, M., O'Connell, C. S., Smith, P., and West, P. C.: Spatially explicit estimates of N_2O emissions from croplands suggest climate mitigation opportunities from improved fertilizer management, Glob. Change Biol., 22, 3383-3394, doi:10.1111/gcb.13341, 2016.

Griffis, T. J., Lee, X., Baker, J. M., Russelle, M. P., Zhang, X., Venterea, R., and Millet, D. B.: Reconciling the differences between top-down and bottom-up estimates of nitrous oxide emissions for the US Corn Belt, Global Biogeochem. Cy., 27, 746-754, doi:10.1002/gbc.20066, 2013.

Griffis, T. J., Chen, Z., Baker, J. M., Wood, J. D., Millet, D. B., Lee, X., Venterea, R. T., and Turner, P. A.: Nitrous oxide emissions are enhanced in a warmer and wetter world, P. Natl. Acad. Sci. USA, 114, 12081-12085, doi:10.1073/pnas.1704552114, 2017.

Hall, B. D., Dutton, G. S., and Elkins, J. W.: The NOAA nitrous oxide standard scale for atmospheric observations, J. Geophys. Res., 112, D09305, doi:10.1029/2006JD007954, 2007.

Halko, N., Martinsson, P. G., and Tropp, J. A.: Finding structure with randomness: Probabilistic algorithms for constructing approximate matrix decompositions, SIAM Rev., 53, 217-288, doi:10.1137/090771806, 2011.

Formatted: Subscript

Henze, D. K., Hakami, A., and Seinfeld, J. H.: Development of the adjoint of GEOS-Chem, Atmos. Chem. Phys., 7, 2413-2433, doi:10.5194/acp-7-2413-2007, 2007.

Hirsch, A. I., Michalak, A. M., Bruhwiler, L. M., Peters, W., Dlugokencky, E. J., and Tans, P. P.: Inverse modeling estimates of the global nitrous oxide surface flux from 1998-2001, Global Biogeochem. Cy., 20, GB1008, doi:10.1029/2004gb002443, 2006.

Huang, J., Golombek, A., Prinn, R., Weiss, R., Fraser, P., Simmonds, P., Dlugokencky, E. J., Hall, B., Elkins, J., Steele, P., Langenfelds, R., Krummel, P., Dutton, G., and Porter, L.: Estimation of regional emissions of nitrous oxide from 1997 to 2005 using multinetwork measurements, a chemical transport model, and an inverse method, J. Geophys. Res., 113, D17313, doi:10.1029/2007jd009381, 2008.

International Fertilizer Association: IFA, http://www. fertilizer.org/statistics (last accessed: 15 June 2016), 2016.

Jin, X., and Gruber, N.: Offsetting the radiative benefit of ocean iron fertilization by enhancing N_2O emissions, Geophys. Res. Lett., 30, 2249, doi:10.1029/2003gl018458, 2003.

Kaminski, T., and Heimann, M.: Inverse modeling of atmospheric carbon dioxide fluxes, Science, 294, U1-U1, 2001.

Kopacz, M., Jacob, D. J., Henze, D. K., Heald, C. L., Streets, D. G., and Zhang, Q.: Comparison of adjoint and analytical Bayesian inversion methods for constraining Asian sources of carbon monoxide using satellite (MOPITT) measurements of CO columns, J. Geophys. Res.-Atmos., 114, D04305, doi:10.1029/2007jd009264, 2009.

Kim, D.-G., Vargas, R., Bond-Lamberty, B., and Turetsky, M. R.: Effects of soil rewetting and thawing on soil gas fluxes: a review of current literature and suggestions for future research, Biogeosciences, 9, 2459-2483, doi:10.5194/bg-9-2459-2012, 2012.

Kort, E. A., Eluszkiewicz, J., Stephens, B. B., Miller, J. B., Gerbig, C., Nehrkorn, T., Daube, B. C., Kaplan, J. O., Houweling, S., and Wofsy, S. C.: Emissions of CH_4 and N_2O over the United States and Canada based on a receptor-oriented modeling framework and COBRA-NA atmospheric observations, Geophys. Res. Lett., 35, doi:10.1029/2008gl034031, 2008.

Kort, E. A., Patra, P. K., Ishijima, K., Daube, B. C., Jimenez, R., Elkins, J., Hurst, D., Moore, F. L., Sweeney, C., and Wofsy, S. C.: Tropospheric distribution and variability of N_2O: Evidence for strong tropical emissions, Geophys. Res. Lett., 38, doi:10.1029/2011gl047612, 2011.

Lambert, A., Read, W. G., Livesey, N. J., Santee, M. L., Manney, G. L., Froidevaux, L., Wu, D. L., Schwartz, M. J., Pumphrey, H. C., Jimenez, C., Nedoluha, G. E., Cofield, R. E., Cuddy, D. T., Daffer, W. H., Drouin, B. J., Fuller, R. A., Jarnot, R. F., Knosp, B. W., Pickett, H. M., Perun, V. S., Snyder, W. V., Stek, P. C., Thurstans, R. P., Wagner, P. A., Waters, J. W., Jucks, K. W., Toon, G. C., Stachnik, R. A., Bernath, P. F., Boone, C. D., Walker, K. A., Urban, J., Murtagh, D., Elkins, J. W., and Atlas, E.: Validation of the Aura Microwave Limb Sounder middle atmosphere water vapor and nitrous oxide measurements, J. Geophys. Res.-Atmos., 112, D24S26, 10.1029/2007jd008724, 2007.

Liu, J. J., Bowman, K. W., Lee, M., Henze, D. K., Bousserez, N., Brix, H., Collatz, G. J., Menemenlis, D., Ott, L., Pawson, S., Jones, D., and Nassar, R.: Carbon monitoring system flux estimation and attribution: impact of ACOS-GOSAT X-CO_2 sampling on the inference of terrestrial biospheric sources and sinks, Tellus B, 66, doi:10.3402/tellusb.v66.22486, 2014.

Liu, J. J., Bowman, K. W., and Henze, D. K.: Source-receptor relationships of column-average CO_2 and implications for the impact of observations on flux inversions, J. Geophys. Res., 120, 5214-5236, doi:10.1002/2014jd022914, 2015.

Manizza, M., Keeling, R. F., and Nevison, C. D.: On the processes controlling the seasonal cycles of the air-sea fluxes of O_2 and N_2O: A modelling study, Tellus B, 64, doi:10.3402/tellusb.v64i0.18429, 2012.

Miller, S. M., Kort, E. A., Hirsch, A. I., Dlugokencky, E. J., Andrews, A. E., Xu, X., Tian, H., Nehrkorn, T., Eluszkiewicz, J., Michalak, A. M., and Wofsy, S. C.: Regional sources of nitrous oxide over the United States: Seasonal variation and spatial distribution, J. Geophys. Res., 117, D06310, doi:10.1029/2011jd016951, 2012.

Mosier, A., Kroeze, C., Nevison, C., Oenema, O., Seitzinger, S., and van Cleemput, O.: Closing the global N(2)O budget: nitrous oxide emissions through the agricultural nitrogen cycle - OECD/IPCC/IEA phase II development of IPCC guidelines for national greenhouse gas inventory methodology, Nutr. Cycl. Agroecosys., 52, 225-248, doi:10.1023/a:1009740530221, 1998.

Myhre, G., Shindell, D., Bréon, F.-M., Collins, W., Fuglestvedt, J., Huang, J., Koch, D., Lamarque, J.-F., Lee, D., Mendoza, B., Nakajima, T., Robock, A., Stephens, G., Takemura, T. and Zhang, H.: Anthropogenic and natural radiative forcing, in: Climate Change 2013: The Physical Science Basis. Contribution of Working Group I to the Fifth Assessment Report of the Intergovernmental Panel on Climate Change, edited by: Stocker, T. F., Qin, D., Plattner, G.-K., Tignor, M., Allen, S. K., Boschung, J., Nauels, A., Xia, Y., Bex, V., Midgley, P. M., Cambridge, United Kingdom, and New York, NY, USA, 2013.

Nevison, C. D., Weiss, R. F., and Erickson, D. J.: Global oceanic emissions of nitrous oxide, J. Geophys. Res.-Oceans, 100, 15809-15820, doi:10.1029/95jc00684, 1995.

Park, S., Croteau, P., Boering, K. A., Etheridge, D. M., Ferretti, D., Fraser, P. J., Kim, K. R., Krummel, P. B., Langenfelds, R. L., van Ommen, T. D., Steele, L. P., and Trudinger, C. M.: Trends and seasonal cycles in the isotopic composition of nitrous oxide since 1940, Nat. Geosci., 5, 261-265, doi:10.1038/ngeo1421, 2012.

Potter, C. S., Matson, P. A., Vitousek, P. M., and Davidson, E. A.: Process modeling of controls on nitrogen trace gas emissions from soils worldwide, J. Geophys. Res.-Atmos., 101, 1361-1377, doi:10.1029/95jd02028, 1996.

Prather, M., Ehhalt, D., Dentener, F., Derwent, R., Dlugokencky, E., Holland, E., Isaksen, I., Katima, J., Kirchhoff, V., Matson, P., Midgley, P., and Wang, M.: Atmospheric chemistry and greenhouse gases, in Climate Change 2011: The Scientific Basis. Third Annual Assessment Report of the Intergovernmental Panel on Climate Change, edited by: Joos, F. and McFarland, M., Cambridge University Press, Cambridge, UK, 239-287, 2001.

Prather, M. J., Holmes, C. D., and Hsu, J.: Reactive greenhouse gas scenarios: Systematic exploration of uncertainties and the role of atmospheric chemistry, Geophy. Res. Lett., 39, L09803, doi:10.1029/2012gl051440, 2012.

Prinn, R. G., Weiss, R. F., Fraser, P. J., Simmonds, P. G., Cunnold, D. M., Alyea, F. N., O'Doherty, S., Salameh, P., Miller, B. R., Huang, J., Wang, R. H. J., Hartley, D. E., Harth, C., Steele, L. P., Sturrock, G., Midgley, P. M., and McCulloch, A.: A history of chemically and radiatively important gases in air deduced from ALE/GAGE/AGAGE, J. Geophys. Res., 105, 17751-17792, doi:10.1029/2000jd900141, 2000.

Ravishankara, A. R., Daniel, J. S., and Portmann, R. W.: Nitrous Oxide (N_2O): The Dominant Ozone-Depleting Substance Emitted in the 21st Century, Science, 326, 123-125, doi:10.1126/science.1176985, 2009.

Saikawa, E., Schlosser, C. A., and Prinn, R. G.: Global modeling of soil nitrous oxide emissions from natural processes, Global Biogeochem. Cy., 27, 972-989, doi:10.1002/gbc.20087, 2013.

Saikawa, E., Prinn, R. G., Dlugokencky, E., Ishijima, K., Dutton, G. S., Hall, B. D., Langenfelds, R., Tohjima, Y., Machida, T., Manizza, M., Rigby, M., O'Doherty, S., Patra, P. K., Harth, C. M., Weiss, R. F., Krummel, P. B., van der Schoot, M., Fraser, P. J., Steele, L. P., Aoki, S., Nakazawa, T., and Elkins, J. W.: Global and regional emissions estimates for N_2O, Atmos. Chem. Phys., 14, 4617-4641, doi:10.5194/acp-14-4617-2014, 2014.

Seitzinger, S. P., and Kroeze, C.: Global distribution of nitrous oxide production and N inputs in freshwater and coastal marine ecosystems, Global Biogeochem. Cy., 12, 93-113, doi:10.1029/97gb03657, 1998.

Shcherbak, I., Millar, N., and Robertson, G. P.: Global metaanalysis of the nonlinear response of soil nitrous oxide (N_2O) emissions to fertilizer nitrogen, P. Natl. Acad. Sci. USA, 111, 9199-9204, doi:10.1073/pnas.1322434111, 2014.

Sokolov, A. P., Stone, P. H., Forest, C. E., Prinn, R., Sarofim, M. C., Webster, M., Saltsev, S., and Schlosser, C. A.: Probabilistic forecast for twenty-first-century climate based on uncertainties in emissions (without policy) and climate parameters, J. Clim. 2, 5175-5204, doi:10.1175/2009JCLI2863.1, 2009.

Spantini, A., Solonen, A., Cui, T. G., Martin, J., Tenorio, L., and Marzouk, Y.: Optimal low-rank approximations of Bayesian linear inverse problems, SIAM J. Sci. Comput., 37, A2451-A2487, doi:10.1137/140977308, 2015.

Thompson, R. L., Bousquet, P., Chevallier, F., Rayner, P. J., and Ciais, P.: Impact of the atmospheric sink and vertical mixing on nitrous oxide fluxes estimated using inversion methods, J. Geophys. Res., 116, D17307, doi:10.1029/2011jd015815, 2011.

Thompson, R. L., Chevallier, F., Crotwell, A. M., Dutton, G., Langenfelds, R. L., Prinn, R. G., Weiss, R. F., Tohjima, Y., Nakazawa, T., Krummel, P. B., Steele, L. P., Fraser, P., O'Doherty, S., Ishijima, K., and Aoki, S.: Nitrous oxide emissions 1999 to 2009 from a global atmospheric inversion, Atmos. Chem. Phys., 14, 1801-1817, doi:10.5194/acp-14-1801-2014, 2014a.

Thompson, R. L., Patra, P. K., Ishijima, K., Saikawa, E., Corazza, M., Karstens, U., Wilson, C., Bergamaschi, P., Dlugokencky, E., Sweeney, C., Prinn, R. G., Weiss, R. F., O'Doherty, S., Fraser, P. J., Steele, L. P., Krummel, P. B., Saunois, M., Chipperfield, M., and Bousquet, P.: TransCom N_2O model inter-comparison - Part 1: Assessing the influence of transport and surface fluxes on tropospheric N_2O variability, Atmos. Chem. Phys., 14, 4349-4368, doi:10.5194/acp-14-4349-2014, 2014b.

Thompson, R. L., Ishijima, K., Saikawa, E., Corazza, M., Karstens, U., Patra, P. K., Bergamaschi, P., Chevallier, F., Dlugokencky, E., Prinn, R. G., Weiss, R. F., O'Doherty, S., Fraser, P. J., Steele, L. P., Krummel, P. B., Vermeulen, A., Tohjima, Y., Jordan, A., Haszpra, L., Steinbacher, M., Van der Laan, S., Aalto, T., Meinhardt, F., Popa, M. E., Moncrieff, J., and Bousquet, P.: TransCom N_2O model inter-comparison - Part 2: Atmospheric inversion estimates of N_2O emissions, Atmos. Chem. Phys., 14, 6177-6194, doi:10.5194/acp-14-6177-2014, 2014c.

Turner, A. J., Jacob, D. J., Wecht, K. J., Maasakkers, J. D., Lundgren, E., Andrews, A. E., Biraud, S. C., Boesch, H., Bowman, K. W., Deutscher, N. M., Dubey, M. K., Griffith, D. W. T., Hase, F., Kuze, A., Notholt, J., Ohyama, H., Parker, R., Payne, V. H., Sussmann, R., Sweeney, C., Velazco, V. A., Warneke, T., Wennberg, P. O., and Wunch, D.: Estimating global and North American methane emissions with high spatial resolution using GOSAT satellite data, Atmos. Chem. Phys., 15, 7049-7069, doi:10.5194/acp-15-7049-2015, 2015.

Turner, P. A., Griffis, T. J., Lee, X. H., Baker, J. M., Venterea, R. T., and Wood, J. D.: Indirect nitrous oxide emissions from streams within the US Corn Belt scale with stream order, P. Natl. Acad. Sci. USA, 112, 9839-9843, doi:10.1073/pnas.1503598112, 2015.

van der Werf, G. R., Randerson, J. T., Giglio, L., Collatz, G. J., Mu, M., Kasibhatla, P. S., Morton, D. C., DeFries, R. S., Jin, Y., and van Leeuwen, T. T.: Global fire emissions and the contribution of deforestation, savanna, forest, agricultural, and peat fires (1997-2009), Atmos. Chem. Phys., 10, 11707-11735, doi:10.5194/acp-10-11707-2010, 2010.

Volk, C. M., Elkins, J. W., Fahey, D. W., Dutton, G. S., Gilligan, J. M., Loewenstein, M., Podolske, J. R., Chan, K. R., and Gunson, M. R.: Evaluation of source gas lifetimes from stratospheric observations, J. Geophys. Res.-Atmos., 102, 25543-25564, 10.1029/97jd02215, 1997.

Wagner-Riddle, C., Congreves, K. A., Abalos, D., Berg, A. A., Brown, S. E., Ambadan, J. T., Gao, X. P., and Tenuta, M.: Globally important nitrous oxide emissions from croplands induced by freeze-thaw cycles, Nat. Geosci., 10, 279-283, doi:10.1038/ngeo2907, 2017.

Wecht, K. J., Jacob, D. J., Sulprizio, M. P., Santoni, G. W., Wofsy, S. C., Parker, R., Bosch, H., and Worden, J.: Spatially resolving methane emissions in California: constraints from the CalNex aircraft campaign and from present (GOSAT, TES) and future (TROPOMI, geostationary) satellite observations, Atmos. Chem. Phys., 14, 8173-8184, doi:10.5194/acp-14-8173-2014, 2014.

Wells, K. C., Millet, D. B., Bousserez, N., Henze, D. K., Chaliyakunnel, S., Griffis, T. J., Luan, Y., Dlugokencky, E. J., Prinn, R. G., O'Doherty, S., Weiss, R. F., Dutton, G. S., Elkins, J. W., Krummel, P. B., Langenfelds, R., Steele, L. P., Kort, E. A., Wofsy, S. C., and Umezawa, T.: Simulation of atmospheric N_2O with GEOS-Chem and its adjoint: evaluation of observational constraints, Geosci. Model Dev., 8, 3179-3198, doi:10.5194/gmd-8-3179-2015, 2015.

Wells, K. C., Millet, D. B., Cady-Pereira, K. E., Shephard, M. W., Henze, D. K., Bousserez, N., Apel, E. C., de Gouw, J., Warneke, C., and Singh, H. B.: Quantifying global terrestrial methanol emissions using observations from the TES satellite sensor, Atmos. Chem. Phys., 14, 2555-2570, doi:10.5194/acp-14-2555-2014, 2014.

Wofsy, S. C.: HIAPER Pole-to-Pole Observations (HIPPO): fine-grained, global-scale measurements of climatically important atmospheric gases and aerosols, Philos. T. Roy. Soc. A, 369, 2073-2086, doi:10.1098/rsta.2010.0313, 2011.

Zhu, C., Byrd, R. H., Lu, P., and Nocedal, J.: L-BFGS-B: a limited memory FORTRAN code for solving bound constrained optimization problems, Tech. rep., Northwestern University, 1994.

Test Name	Observational time range	Sites	Estimation method	Spin-up
MarZonal	1 – 31 March 2010	All	Zonal average, linear interp	One month
AprZonal	25 March – 7 April 2010	All	Zonal average, linear interp	None
AprKriging	25 March – 7 April 2010	All	Kriging	None
AprOpt	1 April – 31 May 2010	All	4D-Var	None
FebOpt	1 February – 31 March 2010	All	4D-Var	Two months
RemoteOpt	1 January – 30 June 2010	Remote[a]	4D-Var	Three months

Table 1: The six initial conditions (for 1 April 2010) tested for N_2O, including the time range of observations used, observation sites included, interpolation or optimization method used, and length of spin-up.

[a]Remote sites include NOAA CCGG sites AZR, CBA, CGO, CHR, CRZ, DRP, GIC, GMI, HBA, ICE, IZO, MID, MLO, PSA, SEY, SHM, SUM, SYO, as well as ship-based measurements taken in the Pacific (POC).

Formatted: Superscript

Formatted: Superscript

Test Name	Bias: All Sites (ppb)			Bias: Northern Hemisphere Sites (ppb)			Bias: Southern Hemisphere Sites (ppb)		
	25th	Median	75th	25th	Median	75th	25th	Median	75th
MarZonal	-0.21	0.30	0.71	0.11	0.46	0.86	-0.66	-0.36	-0.15
AprZonal	-0.13	0.20	0.62	-0.03	0.32	0.73	-0.38	-0.12	0.10
AprKriging	-0.29	0.06	0.42	-0.31	0.02	0.39	-0.20	0.14	0.49
AprOpt	-0.21	0.01	0.21	-0.22	0.01	0.20	-0.21	0.01	0.22
FebOpt	-0.29	0.06	0.48	-0.42	-0.03	0.37	-0.16	0.14	0.39
RemoteOpt	-0.48	-0.14	0.22	-0.44	-0.09	0.33	-0.58	-0.30	-0.04

Table 2: Initial bias statistics for each of the six initial conditions with respect to observations at all sites, Northern Hemisphere sites, and Southern Hemisphere sites. Statistics are calculated for the first week of the simulation (1-7 April 2010).

Region	A priori emissions	A posteriori emissions		
		Standard 4D-Var inversion	Continental-scale inversion	SVD-based inversion
North America	1.61	1.30	1.78	1.24
South America	3.09	3.68	3.58	3.28
Europe	1.70	1.05	0.57	0.43
Africa	2.65	2.97	2.92	2.85
Asia	4.18	4.47	4.59	3.81
Oceania	0.76	0.79	0.64	0.84
Northern oceans (30° - 90° N)	0.66	0.52	0.07	0.15
Tropical oceans (30° S - 30° N)	2.03	2.19	2.99	2.70
Southern oceans (30° - 90° S)	0.79	0.70	0.39	0.53
Global	**17.4**	**17.7**	**17.5**	**15.9**

Table 3: 2011 N_2O emissions (Tg N yr^{-1}) over six continental and three oceanic regions for the a priori database, and a posteriori results for the three inversion frameworks used here.

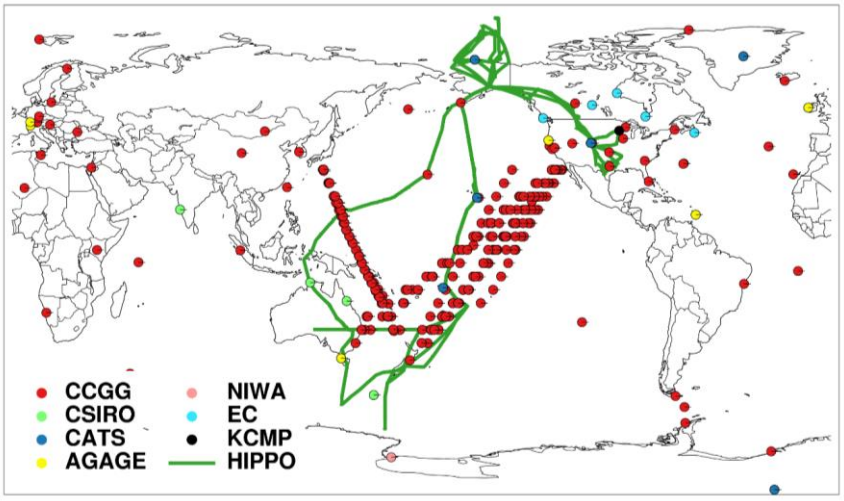

Figure 1: Global surface observing network for atmospheric N_2O. Shown are surface discrete measurement locations for the NOAA Carbon Cycle and Greenhouse Gases (CCGG) network, the Commonwealth Scientific and Industrial Research Organisation (CSIRO) network, the National Institute of Water and Atmospheric Research (NIWA) network, and the Environment Canada (EC) network, as well as semi-continuous measurement locations in the NOAA Chromatograph for Atmospheric Trace Species (CATS) network, the Advanced Global Atmospheric Gases Experiment (AGAGE) network, and the KCMP tall tower site. Also shown are flight tracks from the HIPPO IV and V deployments.

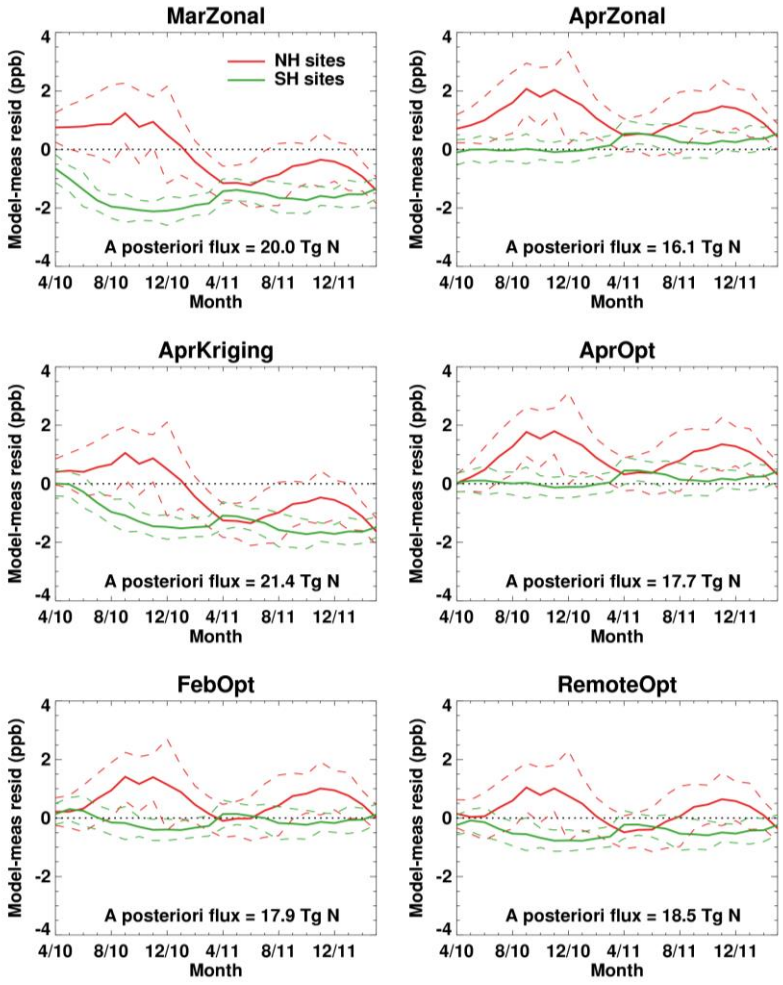

Figure 2: Impact of initial conditions on a two-year (April 2010 to April 2012) N_2O simulation and inversion. Shown are timelines of the model-measurement residuals for a two-year forward-model simulation initialized using each of the six initial conditions listed in Table 1. The solid line represents the mean and the dashed lines represent the standard deviation about the mean for Northern Hemisphere (red) and Southern Hemisphere sites (green). The final 2011 a posteriori global flux for each simulation derived using a standard 4D-Var inversion is noted at the bottom of each panel.

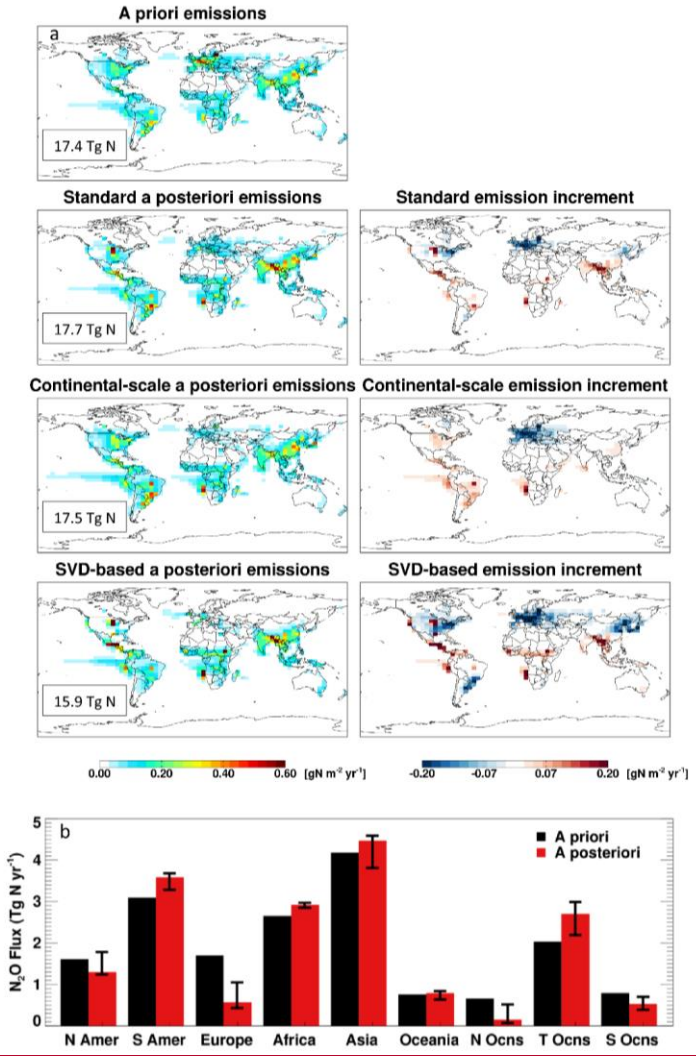

Figure 3: (a) Left panels: 2011 annual N_2O emissions ~~(gN m^{-2} yr^{-1})~~ for the a priori database and a posteriori results for each of the inversion frameworks used here (standard 4D-Var, continental-scale inversion, SVD-based inversion). Global fluxes are shown inset in each map. Right panels: Annual posterior emission increments relative to the a priori database for each inversion framework. (b) 2011 annual N_2O flux ~~(Tg N yr^{-1})~~ over six continental and three oceanic regions for the a priori database (black),

and the a posteriori median from the three inversion frameworks (red). Error bars denote the range of a posteriori values for each region.

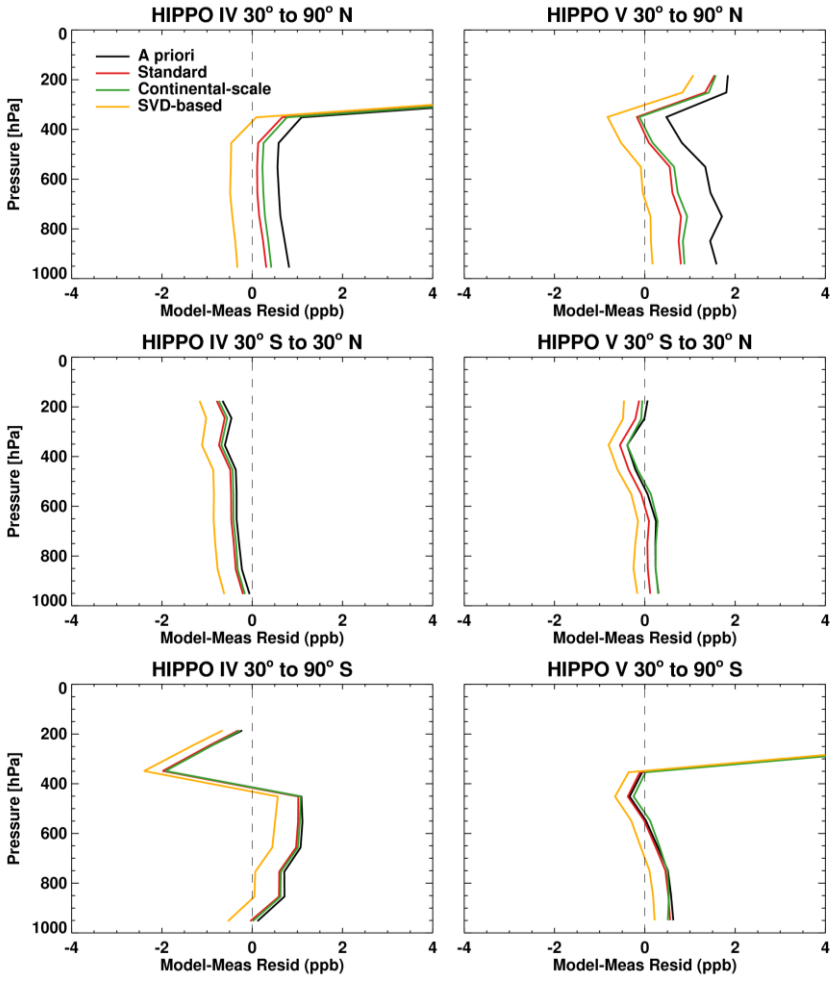

Figure 4: A posteriori evaluation of N_2O inversion results using HIPPO data (not themselves used in the inversion). Shown are ~~average~~ mean vertical profiles of the model-measurement difference for HIPPO IV (14 June-11 July 2011, left column) and

HIPPO V (9 August-9 September 2011, right column) as a function of latitude. A priori results are shown in black and a posteriori results in red (standard 4D-Var inversion), green (continental inversion), and gold (SVD-based inversion).

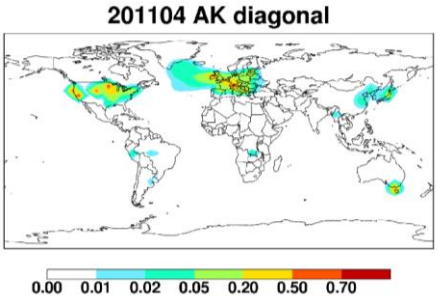

Figure 5: Averaging kernel diagonal values for April 2011 in the SVD-based inversion, calculated from Eq. (4).

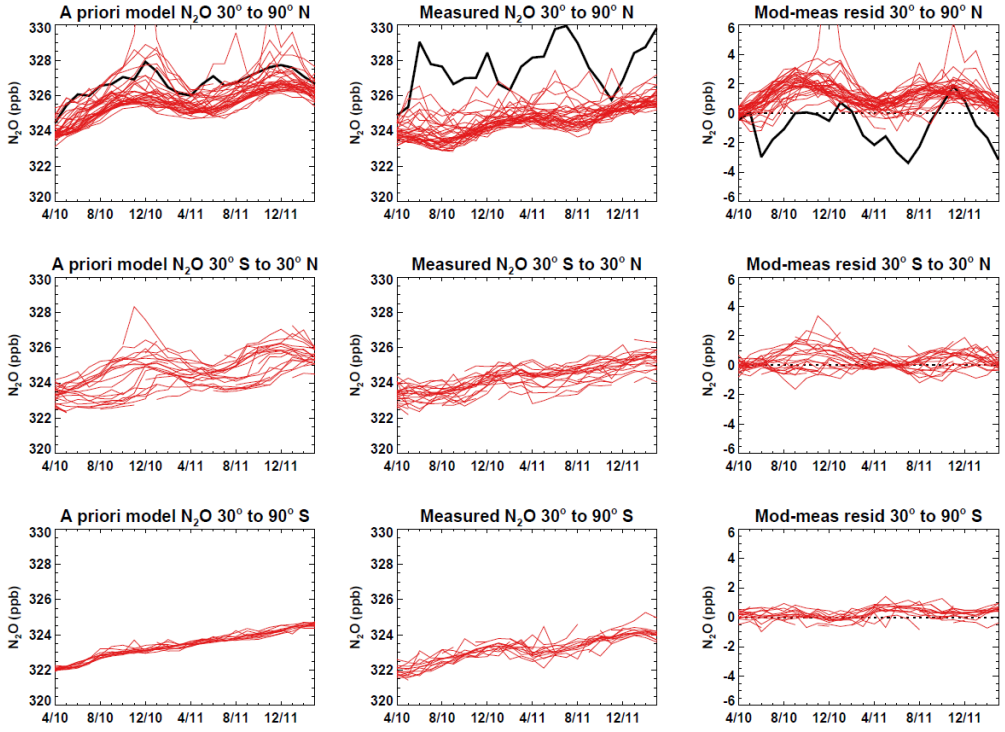

Figure 6: Two-year timelines of monthly-averaged a priori modeled and measured N_2O mixing ratios, and the resulting model-measurement residuals, for individual measurement sites as a function of latitude. The solid black line in the top panels shows results for the KCMP tall tower site in ~~Minnesota~~MN, USA.

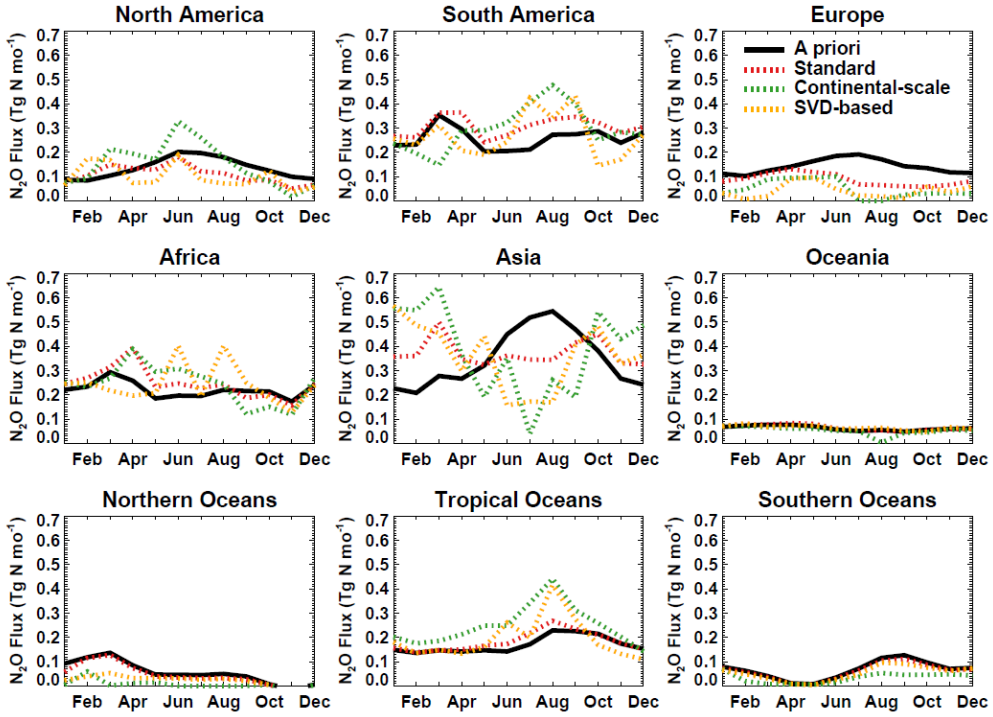

Figure 7: Monthly N_2O emissions ~~(Tg N month^{-1})~~ for 2011 over six continental and three oceanic regions. Shown is the a priori database (black)~~,~~ and a posteriori results for the standard 4D-Var inversion (red), the continental-scale inversion (green), and the SVD-based inversion (gold).